Aus dem Institut für Radiologie
der Medizinischen Fakultät Charité – Universitätsmedizin Berlin

DISSERTATION

Validierung interventionell radiologischer Thermoablationsverfahren und ihre Visualisierung in der offenen 1 Tesla Magnetresonanztomographie

zur Erlangung des akademischen Grades
Doctor medicinae (Dr. med.)

vorgelegt der Medizinischen Fakultät
Charité – Universitätsmedizin Berlin

von

Hendrik Gabriel Rathke

aus Sindelfingen

Datum der Promotion: 08.12.2017

INHALT

ABKÜRZUNGSVERZEICHNIS

BCLC	Barcelona Clinic Liver Cancer Classification
Bzw.	Beziehungsweise
°C	Grad Celsius
CT	Computertomographie
EM	Elektromagnetisch
EWS	Philips Extended Work Space
HCC	Hepatozelluläres Karzinom
HFO	High Field Open (offenes Hochfeld-MRT)
IR	Inversionsumkehr (MRT)
kHz	Kilo-Hertz
LITT	Laser-induzierte Thermotherapie
MHz	Mega-Hertz
Min	Minuten
MPR	Multiplanare Rekonstruktion
MRT / MRI	Magnetresonanztomographie
Ms	Millisekunden
MWA	Mikrowellenablation
NADPH	Nicotinsäureamid-Adenin-Dinukleotid-Hydridion-Phosphat
PD	Protonendichte gewichtete Sequenz
RFA	Radiofrequenzablation
S, sec	Sekunden
Sog.	So genannt
SPSS	Statistical Package for Social Sciences
T	Tesla
TACE	Transarterielle Chemoembolisation
TE	Time of Echo (MRT)
TR	Time of Repetition (MRT)
TSE	Turbo Spin Echo (MRT)
TZ	Transitionalzone
U.a.	Unter anderem
US	Ultraschall
W	Watt

ZUSAMMENFASSUNG

Einführung:

Thermoablationsverfahren wie die Radiofrequenzablation und Mikrowellenablation werden in der Therapie von Primärtumoren und Metastasen in Organen und Knochen eingesetzt. Die initial vollständige Tumorablation ist für die weitere Prognose der Erkrankung von besonderer Bedeutung. Hierfür ist die möglichst frühzeitige Kenntnis wichtig, ob die Ablation vollständig ist oder ob Teile des zu therapierenden Areals einer weiteren Intervention bedürfen. In dieser Arbeit wurde u.a. untersucht, wie die Ausdehnung des Ablationsareals direkt nach der Intervention in einem offenen 1 T MRT ersichtlich war und insbesondere ob der Randbereich der Ablationszone beurteilt werden konnte.

Bei der Mikrowellenablation können mit einer einzelnen Elektrode auf Grund der Reichweite der elektromagnetischen Wellen im Gewebe nur kleinere Tumorherde therapiert werden. Diverse Studien mit der RFA haben gezeigt, dass sich das Ablationsvolumen mittels Flüssigkeitsinjektion vergrößern ließ. Ein Studienziel dieser Arbeit bestand in der Evaluation, ob Flüssigkeitsinjektionen vor der MWA mit unterschiedlichen Natrium-Ionenkonzentrationen ähnlich zu einer Vergrößerung des Ablationsareals führen konnten wie mit der RFA.

Methodik:

In dieser Rahmenschrift wurden zwei Originalarbeiten für die Radiofrequenzablation sowie eine Originalarbeit zur Mikrowellenablation zusammengefasst. Zuerst wurden die Arbeiten zur RFA gemeinsam vorgestellt und anschließend die Arbeit zur MWA.

Ergebnisse:

Für die Arbeiten der RFA zeigte sich, dass alle Systeme das Zielvolumen der 3 cm-Läsionen von 14,14 cm^3 übertrafen. Die Ergebnisse für die 5 cm-Läsionen mit einem Zielvolumen von 65,45 cm^3 zeigten ein gemischtes Bild: Die Systeme von Boston Scientific und Celon übertrafen das Zielvolumen, die Systeme von Radionics und AngioDynamics blieben unterhalb des Zielvolumens.

Im MRT zeigten sich bei allen Läsionsgrößen und Serien kleinere Volumina als in der makroskopischen Messung. Gemittelt über alle vier RFA-Systeme und Läsionsgrößen waren etwa 60 % des Ablationsvolumens im MRT mit den untersuchten Sequenzen nicht sichtbar.

In den Versuchen zur Mikrowellenablation zeigte sich kein signifikanter Unterschied zwischen den Versuchsreihen mit iso- oder hypertoner NaCl-Lösung im Vergleich zu der Versuchsreihe mit Wasser oder der Versuchsreihe ohne Flüssigkeitsinjektion.

Diskussion:

Im Vergleich der beiden verschiedenen Sequenzen zeigten sich sowohl für die RFA als auch die MWA größer visualisierte Ablationsvolumina mit der T1-Sequenz im Vergleich zur PD-Sequenz. Allerdings konnte mit den gewählten Sequenzen der Übergang von Transitionalzone zu gesundem Gewebe nicht abschließend beurteilt werden. Somit konnte unmittelbar nach der Intervention keine abschließende Aussage über die Vollständigkeit der Ablation allein aus der MR-Visualisierung getroffen werden.

Mit den Versuchen der Mikrowellenablation zeigte sich, dass, im Gegensatz zu entsprechenden RFA-Versuchen, eine Flüssigkeitsinjektion vor der Intervention in das Gewebe, gleich welcher Natrium-Konzentration, nicht zu einer Vergrößerung des Ablationsareals führte. Zu einer Vergrößerung des Ablationsareals musste die MW-Antenne entweder repositioniert oder mit mehreren Elektroden gleichzeitig therapiert werden.

ABSTRACT

Introduction:

Thermal ablation techniques like RFA and MWA became a therapy option for primary and secondary malignancies in organs and bones. An entire tumor ablation directly after intervention is crucial for the further course of the disease. Therefore, an image validation right after intervention should ratify whether the ablation was sufficient or further therapy is mandatory. One aim of this thesis was to evaluate if the entire thermal ablation necrosis, especially the border from ablated to healthy tissue, was visible directly after intervention in an open 1 T MRI system.

For the MWA using a single antenna, only smaller necroses can be produced because of the limited range of microwaves in tissue. Several RFA-studies reported possible enlargement of necroses by installing sodium solutions into tissue previous to RFA. One aim of this thesis was to investigate whether preinterventional fluid injection before MWA might enlarge the necrosis similarly to fluid injection performing RFA.

Methods:

In this thesis, two original scientific articles for RFA and one original scientific article on MWA were summarized. Therefore, the articles related to RFA were presented together. Subsequently the MWA article was presented.

Results:

For the 3 cm ablation all tested RF systems exceeded the target volume of 14.14 cm^3. For the 5 cm lesion only the Boston Scientific and the Celon system exceeded the target volume of 65.45 cm^3. The Radionics and AngioDynamics system achieved smaller ablation volumes and remained below the target volume.

For the MR-volumetry all volumes for every test series and lesion size were smaller than the macroscopically measured and calculated volumes. Averaged over all four RFA-systems, lesion sizes and sequences, 60 % of the necrosis zone after Intervention was not visible.

For MWA no significant differences were detected between the test series including fluid preinjection of iso- or hypertonic saline solutions in comparison to the trials without preinjection or only water-injection.

Discussion:

After evaluation of the two MR sequences, in both RFA and MWA-trials the T1-sequence detected larger ablation-volumes than the PD-sequence. However, the border from the transitional zone to healthy tissue was not detectable by MRI with the respective sequences directly after intervention. Therefore, no accurate statement about the completeness of the thermal ablation by MR-imaging could be given.

For MWA, fluid preinjection did not enlarge the necrosis in contrast to RFA, irrespective of sodium concentration in water. Therefore larger ablations volumes needed a repositioning of the MW-antenna or the simultaneous use of more than one MW-system.

EINFÜHRUNG

Das hepatozelluläre Karzinom (HCC) ist der häufigste Leber-Primärtumor; etwa 80 bis 85 % der primären Lebertumoren weltweit werden dieser Tumorentität zugeschrieben (1). Auf Grund der hohen Letalität ist das HCC die zweithäufigste tumorassoziierte Todesursache weltweit (2). Insbesondere in Entwicklungsländern kommt es zu einer erhöhten Fallzahl: 83 % der neu aufgetretenen HCC-Fälle, geschätzt 782.000 Neuerkrankungen im Jahr 2012, wurden in weniger entwickelten Ländern diagnostiziert (1).
In der Europäischen Union zeigte sich ein inhomogenes Bild mit einer berechneten Inzidenz in Nordeuropa mit 4,6/100.000 (Niederlande) im Vergleich zu 11,3/100.000 in Frankreich für die männliche Bevölkerung für das Jahr 2012. Das HCC weist eine Geschlechtstendenz auf. Die berechnete Inzidenz für Frauen liegt deutlich unterhalb der für Männer (exemplarisch hierfür die Niederlande mit einer berechneten Inzidenz für Frauen von 0,4/100.000) (1, 2). Die typische Präkanzerose ist die Leberzirrhose, die bei 80–90 % der HCC-Fälle diagnostiziert wird (3).

In-vivo-Thermoablationsverfahren wie die RFA und die MWA werden in der Therapie von Primärtumoren und Metastasen in Organen und Knochen eingesetzt. Ein besonders weit verbreitetes Einsatzgebiet dieser Therapiemodalitäten sind Leber-Malignome (4-6).

Bei klinischer Indikation und anästhesiologischer Tauglichkeit wird häufig bei kleinen oder lokal begrenzten Tumorsituationen eine chirurgische Intervention bevorzugt. Allerdings sind nur 20 bis 30 Prozent aller HCC-Patienten für eine Leberteilresektion oder Transplantation geeignet (7). Daher wird für die weit größere Patientenzahl eine weitere Therapieoption und –strategie benötigt. Entsprechend der Barcelona Clinic Liver Cancer (BCLC) Klassifikation können interventionelle Therapieverfahren wie die RFA bereits in einem relativ frühen Stadium der Erkrankung zum Einsatz kommen. (8, 9)

Hocquelet et al. haben in einer Studie mit dem Vergleich zwischen der chirurgischen Resektion eines HCC und der Therapie mittels RFA bei 281 Patienten gezeigt, dass sich keine wesentlichen Unterschiede bei Gesamtüberleben und krankheitsfreier Überlebenszeit darstellen ließen (5). Im RFA-Therapiearm waren sowohl Hospitalisationsdauer als auch die Komplikationsrate niedriger (5). Eine Kombination der RFA mit anderen interventionellen Therapieverfahren wie der LITT, TACE oder Immuntherapie kann den positiven Effekt möglicherweise noch verstärken (10).

Ziel der Thermoablation ist die mikroinvasive, vollständige Zerstörung des Tumorgewebes zuzüglich eines zirkumferenten Sicherheitssaumes von 0,5 cm. Dieser Sicherheitssaum dient der Zerstörung möglicher befallener Zellen außerhalb des erkennbaren Tumorherdes. Kim et al. zeigten in einer retrospektiven Studie, dass bereits ein Abstand von 3 mm ausreichen würde, um einen lokalen Tumorprogress zu minimieren (11). Die initial vollständige Tumorablation nach einer Intervention ist ein entscheidender Parameter für den weiteren Krankheitsverlauf (12).

Patientenindividuelle Risikofaktoren wie die Lagebeziehung zu großen Gefäßen sowie Gewebeeigenschaften müssen für die Auswahl der jeweiligen Therapiemodalität mit entsprechenden Elektroden für die Ablation mit einbezogen werden. Herstellerspezifische Ablationsprotokolle bieten einen Anhaltspunkt für die Wahl der Elektrode sowie für die Ablationsdauer. Die nahe Lagebeziehung eines Tumors zu großen Gefäßen kann zu einer geringeren Erwärmung des Gewebes (Kühlung des Gewebes durch den Blutfluss = Heat-Sink-Effekt) und somit zu einer inkompletten Ablation führen (13, 14). Gewebeeigenschaften wie eine erhöhte Impedanz (Widerstand bei Wechselstrom), beispielsweise im Rahmen einer Leberzirrhose mit einer möglicherweise daraus resultierenden geringeren Energieabgabe in das Gewebe, müssen ebenfalls berücksichtigt werden (4).

Daher wird die Intervention mittels bildgebender Verfahren wie Ultraschall, Computertomographie und Magnetresonanztomographie durchgeführt und das Ablationsareal vor, während und nach der Intervention anhand von Größe, Form und zeitlicher Dynamik (insbesondere Größenprogredienz /-regredienz im Verlauf) beurteilt (15). Nach einer therapeutischen Intervention ist es in der Regel nicht möglich, das abladierte Leberparenchym makroskopisch oder histologisch bezüglich des tumorfreien Sicherheitssaums zu untersuchen.

Die frühzeitige Aussage über die Vollständigkeit der Ablation unter Schonung des tumorfreien Leberparenchyms kann somit helfen, die Tumorablation möglichst valide beurteilen zu können und weitere Eingriffe nach Möglichkeit zu verhindern (16).

METHODIK

ZIELSTELLUNG

In dieser Rahmenschrift wurden zuerst zwei Originalarbeiten zur RFA (**Publikationen I und II**) und anschließend eine Originalarbeit zur MWA (**Publikation III**) zusammengeführt. Die weiteren Arbeiten wurden in der kompletten Publikationsliste aufgeführt.

Ein Ziel dieser Dissertation war der Vergleich von Ablationsverfahren wie der RFA und der MWA in einem offenen 1 T MRT. Hierfür wurden die Ziele in verschiedene Teil-Fragestellungen gegliedert. Ein Ziel war ein standardisierter Vergleich zwischen vier frei verkäuflichen RFA-Systemen. Zwei verschiedene Zielvolumina wurden für alle vier Systeme definiert und die entstandenen Läsionen sowohl makroskopisch als auch MR-volumetrisch evaluiert. Eine weitere Zielstellung war die Beurteilung des Randbereichs der Ablationszone im offenen MRT direkt nach der Intervention bezüglich ihrer jeweiligen Abgrenzbarkeit zum umliegenden gesunden Gewebe im Vergleich zum makroskopisch gemessenen Volumen.

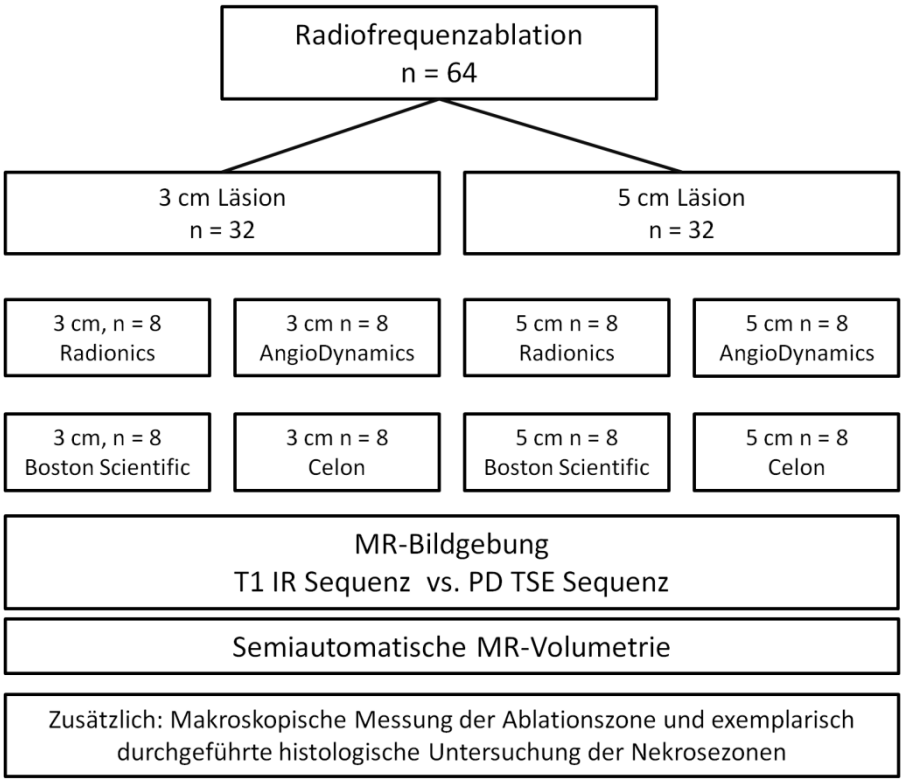

Abbildung 1 – Organigramm Radiofrequenzablation: Jeweils 32 Proben wurden für die zwei verschiedenen Läsionsgrößen verwendet. Für jeden/jedes Hersteller/System wurden bei der entsprechenden Läsion n = 8 Versuche durchgeführt. Nach der Ablation wurden die Proben im offenen MRT mit zwei verschiedenen Sequenzen gescannt. Anschließend erfolgten die makroskopische Messung des Ablationsareals und die Berechnung des Ablationsvolumens. Der MR-Datensatz wurde anhand der zwei Sequenzen mittels semiautomatischer Volumetrie bearbeitet und die entsprechenden Volumina von der EWS-Software berechnet. Exemplarisch erfolgte an einer Probe eine histopathologische Aufarbeitung.

In der **Publikation I** *» Comparison of four radiofrequency ablation systems at two target volumes in an ex vivo bovine liver model. Diagn Interv Radiol. 2014;20(3):251-8 «* wurden vier verschiedene RFA-Systeme unter den gleichen, standardisierten Ausgangsbedingungen getestet. Da zum Zeitpunkt der Versuchsdurchführung lediglich zwei von vier Herstellern MR-kompatible Elektroden zur Verfügung stellten, wurden sämtliche Ablationen für die 3 cm und die 5 cm Zielläsionen der jeweiligen vier Ablationssysteme im MRT-Vorraum durchgeführt, dann gescannt und anschließend auch per makroskopischer Schnitte evaluiert.

Nach erfolgter Ablation wurden die Proben im offenen 1 T MRT mittels zweier angepasster Sequenzen untersucht. Es wurde der Frage nachgegangen, welche Sequenz für die Beurteilung des Lebergewebes besser geeignet war und welche Anteile der Nekrose im Gewebe mittels MR-Bildgebung sichtbar waren. Die Ergebnisse wurden in der **Publikation II** *» Volume comparison of radiofrequency ablation at 3- and 5-cm target volumes for four different radiofrequency generators: MR volumetry in an open 1-T MRI system versus macroscopic measurement. Biomed Tech (Berl). 2015;60(6):521-31. «* veröffentlicht.

Im Anschluss erfolgten die Aufbereitung der Leberproben und deren makroskopische Messung in drei Achsen. Daraufhin sollte eine Untersuchung des Ablationsareals mit Hilfe der NADPH-Diaphorase durchgeführt werden, um die Vitalität des Lebergewebes in der Transitionalzone zu untersuchen (17). Auf Grund von möglichen Störeinflüssen (ex-vivo-Gewebe) wurde dies nicht durchgeführt und anstelle dessen eine Probe in Zusammenarbeit mit dem Institut für Pathologie aufgearbeitet, indem die drei verschiedenen Nekrosezonen innerhalb des Ablationsareals exemplarisch histopathologisch untersucht wurden. Ziel dieser Untersuchung war es eine Aussage über die Vitalität beziehungsweise Zelldestruktion im Außenbereich der Nekrosezone zu erhalten und bei einer Diskrepanz zwischen MR-Volumen und makroskopischen Volumen eine Aussage über die Zugehörigkeit zu „gesundem“ oder „abladiertem“ Gewebe treffen zu können. Die Ergebnisse wurden ebenfalls in der **Publikation II** veröffentlicht.

Die Mikrowellenablation (MWA) im MRT stellte ein im Vergleich zur RFA neueres Ablationsverfahren dar. Da die maximalen Ablationsvolumina des verwendeten MWA-Systems zum Zeitpunkt der Versuchsdurchführung etwa 8 cm^3 betrugen, war eine weitere Zielstellung dieser Dissertation, eine Möglichkeit zur Vergrößerung der Mikrowellenablation zu suchen und zu evaluieren.

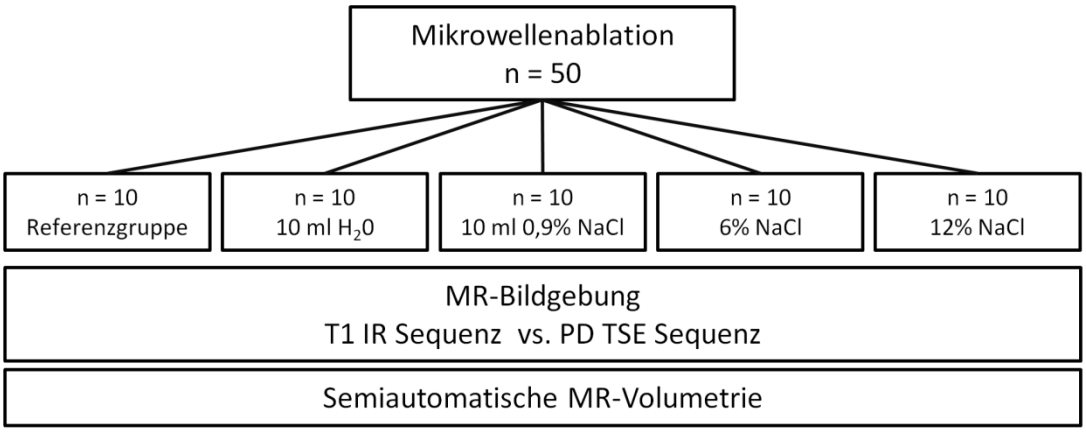

Abbildung 2 – Organigramm Mikrowellenablation: Insgesamt wurden n = 50 Proben für den Versuch verwendet. Verschiedene Lösungen mit unterschiedlicher NaCl-Konzentrationen bzw. H_2O wurden in das Gewebe injiziert. Als Referenzgruppe diente eine Probenreihe ohne Flüssigkeitsinjektion vor der Ablation. Die Proben wurden anschließend im MRT untersucht und mittels semiautomatischer Volumenberechnung analysiert.

In der **Publikation III** *» Fluid preinjection for microwave ablation in an ex vivo bovine liver model assessed with volumetry in an open MRI system. Diagn Interv Radiol. 2013;19(5):427-32.«* wurde der Frage nachgegangen, ob das MWA-Ablationsvolumen vergrößert werden kann, indem, entsprechend bereits in der Fachliteratur publizierter RFA-Versuche, vor der Intervention Flüssigkeiten verschiedener Natrium-Ionenkonzentrationen im Zielgewebe injiziert wurden (18). Für diese Versuchsreihen wurden verschiedene Konzentrationen von NaCl-Lösungen mit einer Probenreihe mit lediglich Wasserinjektion (Aqua ad iniectabilia, B. Braun, Melsungen, Deutschland) sowie einer Referenzgruppe ohne vorherige Flüssigkeitsinjektion miteinander verglichen. Das MRT-Protokoll wurde entsprechend der Versuche der RFA (siehe **Publikation II**) durchgeführt.

RADIOFREQUENZABLATION

VERSUCHSAUFBAU

In den **Publikationen I und II** wurden 64 Versuche in frischer ex-vivo Rinderleber mit Proben von etwa 10x10x10 cm durchgeführt (siehe **Abbildung 1**). Die Proben wurden eine Stunde vor Untersuchungsbeginn langsam auf 37 °C erwärmt. Die Ablationen wurden in einem Wasserbad bei 37 °C in 0,9 % physiologischer Kochsalzlösung durchgeführt. Nach der Ablation wurde die Probe für etwa 10 min bei Raumtemperatur aufbewahrt. Anschließend erfolgte die Untersuchung im 1 T offenen MRT mit zwei verschiedenen Sequenzen, gefolgt von der makroskopischen Präparation und Aufarbeitung der Leberproben.

Geräteeigenschaften

Unter Radiofrequenzablation versteht man die lokale, in das Zielgewebe abgegebene Hochfrequenzenergie im Bereich von 365 bis 480 kHz (siehe Abbildung 3) (19). Über eine Elektrode, die in der Regel perkutan unter Ultraschall-, CT- oder MRT-Kontrolle eingebracht wird, erfolgt die Applikation des Hochfrequenzstroms. Für die Funktion benötigt man einen geschlossenen elektrischen Kreis zwischen dem Applikator (= Elektrode) und der Gegenelektrode (= Ableitungspad) beim monopolaren System oder zwischen zwei oder mehreren Elektroden beim bipolaren System. Da beim bipolaren System der Strom zwischen den jeweiligen Elektroden fließt, benötigt man hier keine Gegenelektrode.

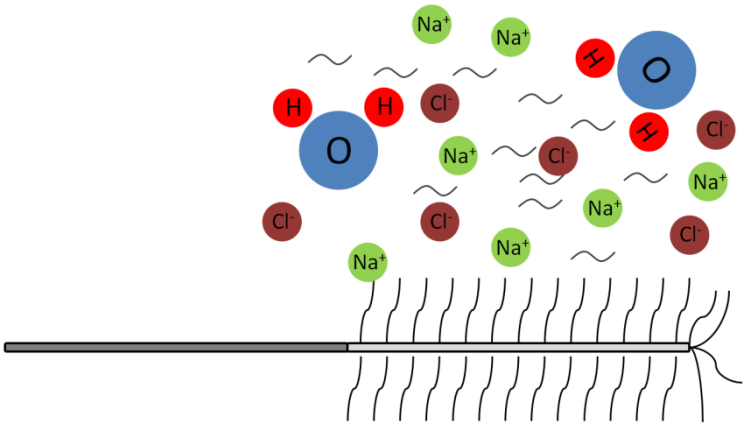

Abbildung 3 - Grundlagen der Radiofrequenzablation: Die Elektrode (grau) liegt im Parenchym. Der Stromkreis wird entweder über die Gegenelektrode auf dem Oberschenkel oder bei bipolaren Elektroden ohne Gegenelektrode geschlossen. Auf Grund von Reibung (Friktionswärme) zwischen Natrium-Ionen kommt es zur Erwärmung des Gewebes. Die Gewebetemperatur liegt an der Elektrode bei etwa 100 °C. Die Temperatur nimmt nach außen konzentrisch ab.

Radionics Cool Tip von Covidien (Mansfield, MA, USA)

Die Ablationszeiten für das Radionics System betrugen für beide Läsionsgrößen jeweils 12 min. Für die 3 cm-Läsionen wurde die Radionics Cool-Tip-Elektrode verwendet. Für die 5 cm-Läsionen wurde die Radionics Cluster-Elektrode, bestehend aus drei einzelnen Elektroden verwendet. Hierbei ist anzumerken, dass die Cluster-Elektrode von Radionics zum Zeitpunkt der Versuche nicht mehr für einen Ablationsdurchmesser von 5 cm zugelassen war. Die maximale, vom Hersteller angegebene Ablationsgröße betrug 4,2 x 4,6 cm. Da die Cluster-Elektrode allerdings eine häufige klinische Anwendung für diese Läsionsgröße fand, wurde sie für die 5 cm-Läsionsgröße mit aufgeführt.

1500X RF von AngioDynamics (Latham, NY, USA)

Das 1500X RF System von AngioDynamics arbeitete im Gegensatz zu den drei anderen Herstellern mit einer temperaturgesteuerten Energiezufuhr. Dem System wurde die gewünschte Zieltemperatur im Gewebe vorgegeben und Temperatursonden, die in die Elektrodennadeln integriert waren, steuerten die Energieabgabe.

Entsprechend der Hersteller-Protokolle wurden für die 3 cm-Läsionen eine Leistung von 150 W, eine Zieltemperatur von 105 °C und eine Ablationszeit von 9 Minuten voreingestellt. Für die 5 cm-Läsionen wurden eine Leistung von 150 W, eine Zieltemperatur von 105 °C und eine Ablationsdauer von 15 Minuten vorgegeben.

RF 3000 von Boston Scientific (Marlborough, MA, USA)

Für die 3 cm-Läsionen wurde entsprechend des Herstellerprotokolls mit einer Ausgangsleistung von 40 W begonnen. Diese wurde alle 30 s um 10 W bis zu einer maximalen Ausgabeleistung von 90 W erhöht. Kam es vor Erreichen der 90 W zu einem Anstieg der Impedanz mit einer Verminderung der Energieabgabe in das Gewebe (sog. Roll-Off), wurde die Stromzufuhr für 30 s pausiert und danach bei der halben Ausgabeleistung, bei der es zum Roll-Off kam, erneut gestartet.

Bei den 5 cm-Läsionen betrug die Ausgangsleistung initial 90 W. Sie wurde alle 30 s um 10 W erhöht, bis die Maximalleistung von 150 W erreicht wurde. Im Falle eines Roll-Off wurde analog zu den 3 cm-Läsionen nach 30 s Pause die Ablation erneut bei 50 % der Ausgabeleistung gestartet.

Celon Power Lab von Celon (Olympus, Shinjuku, Tokyo, Japan)

Das Celon System arbeitet als einziges hier verwendetes System bipolar beziehungsweise multipolar.

Bei den 3 cm-Läsionen wurden zwei Elektroden im Abstand von 1 cm zueinander in der Leber platziert. Die aktive, das heißt unisolierte, Elektrodenlänge betrug 3 cm (Celon ProSurge T30). Die maximale Ausgabeleistung betrug 60 W über eine Zeit von 20 min.

Bei den 5 cm-Läsionen wurden drei Elektroden in einem Dreieck mit einem Abstand von 2,5 cm zueinander in der Leber platziert. Es wurden drei gleiche Elektroden mit einer aktiven Elektrodenspitze von 4 cm verwendet (Celon ProSurge T40). Die maximale Ausgabeleistung betrug 120 W über eine Zeit von 40 min.

MIKROWELLENABLATION

VERSUCHSAUFBAU

In **Publikation III** wurden 50 Versuche in ex-vivo Rinderlebern in Proben von mindestens 8x8x8 cm durchgeführt (siehe Abbildung 2). Für die Versuche wurden die Proben in einem Wasserbad auf 37°C erwärmt und für die Ablation in einer Nierenschale platziert. Insgesamt wurden fünf Serien mit jeweils 10 Leberproben durchgeführt. Nach der Ablation erfolgte die Untersuchung der Proben im 1 T offenen MRT.

GERÄTEEIGENSCHAFTEN

Das System Evident von Covidien (Mansfield, MA, USA) bestand aus einem Generator und einer Antenne (= Ablationsnadel) sowie einer Pumpe zur Kühlung der Elektrode. Die Antenne transportiert die Energie in Form von elektromagnetischen Wellen bei einer Frequenz bis 915 MHz in das Gewebe (siehe Abbildung 4). Die Leistung des Generators wurde für die Versuche entsprechend der Herstellervorgaben auf 45 W bei einer Ablationsdauer von 7 min eingestellt. Verwendet wurde eine 2,0 cm Antenne, um ein Ablationsareal von 8 cm^3 zu produzieren.

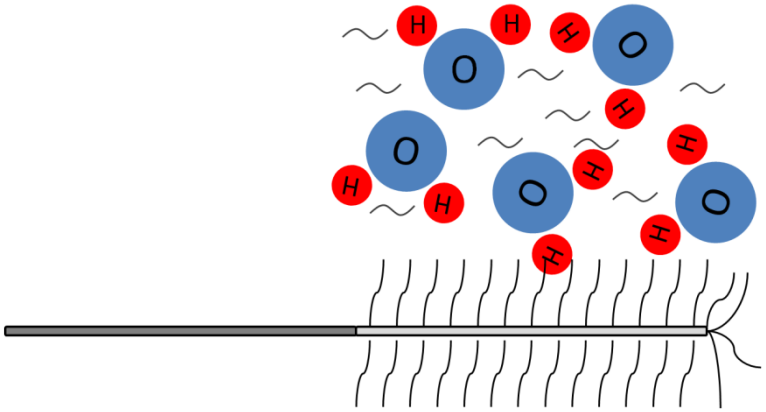

Abbildung 4 – Grundlagen der Mikrowellenablation: Bei der Mikrowellenablation kommt es zur direkten Erwärmung von Wasser mittels Oszillation durch Mikrowellen bei einer Frequenz bis 915 MHz. Wenn die Wassermoleküle (elektrischer Dipol) aus der Phase geraten, wird ein Teil der elektromagnetischen Energie in Wärme umgewandelt.

MAGNETRESONANZTOMOGRAPHIE

Die Leberproben wurden etwa 10 bis 15 min nach der Ablation untersucht, um eine relative Homogenität der Temperatur zwischen Ablationsgewebe und unbehandeltem, umgebenem Gewebe herzustellen. Als Scanner diente ein 1 T offener MRT (Panorama HFO, Best, Niederlande) mit zwei verschiedenen Sequenzen: Eine T1-gewichtete TSE Sequenz mit einer Inversionsumkehr (IR). Die Inversionsumkehr wurde verwendet, um den Kontrast von langen und kurzen T1-Signalen umzukehren – lange T1-Signale erscheinen dementsprechend in den

Bildern hell. Als zweite Sequenz diente eine angepasste „pseudo“ Protonen-Dichte (PD) gewichtete TSE-Sequenz. Die Bezeichnung „pseudo“ erfolgte auf Grund der für das Rinderlebergewebe angepassten langen Relaxationszeit (TR) von 1800 ms, welche (formal) in Richtung einer T2-Sequenz tendierte (Details siehe Table 1 in **Publikation II**). Alle Proben wurden in einer Kniespule „knee-coil“ zentral im Scanner platziert.

Die MR-Datensätze wurden an der Extended-MR-Workspace (EWS) nach der multiplanaren Rekonstruktion (MPR) für die semiautomatische volumetrische Berechnung beziehungsweise Diametermessungen bearbeitet. Als Software diente die *EWS Software Version 2.6.3.2* (Philips Medical Systems, Best, Niederlande, 2009).

MAKROSKOPISCHE MESSUNG DES ABLATIONSVOLUMENS

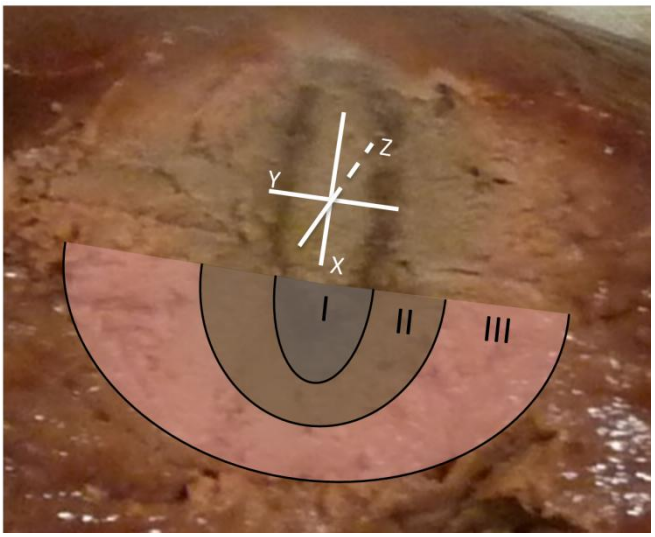

Abbildung 5 – Auswertung der makroskopischen Messung: Die Leberproben wurde entlang der Elektrodeneinstichstelle aufgeschnitten und entsprechend der Dimensionen (weißes Schema, Bildmitte) in den entsprechenden Achsen gemessen. Die Nekrosezone wurde unterteilt in Zone I (Karbonisationszone), Zone II (Koagulationszone) und Zone III (Transitionalzone = TZ). Nach außen schließt sich das nichtabladierte Lebergewebe an. Abbildung aus **Publikation II** (20)

STATISTIK

Die Rohdatensammlung erfolgte mittels Software *Microsoft Excel Version 2007* (Microsoft, Redmond, WA, USA). Die statistische Analyse wurde mit der Software *IBM Statistical Package for Social Sciences* (SPSS) Version 19.0.0.1 (IBM, Armonk, NY, USA) durchgeführt.

Eine vorherige Berechnung der Fallgruppenzahlen wurde gemeinsam mit dem Institut für Biometrie der Charité durchgeführt, ebenso die Beratung über die statistischen Testverfahren. Die statistischen Testverfahren wurden in den jeweiligen Publikationen einzeln und detailliert aufgeführt. Die Daten wurden als Mittelwert ± Standardabweichung präsentiert. Das statistische Signifikanzniveau lag bei $p \leq 0{,}05$.

ERGEBNISSE

RADIOFREQUENZABLATION

Die hier vorgestellten Ergebnisse wurden in den **Publikationen I und II (20, 21)** veröffentlicht. In dieser Rahmenschrift konnten auf Grund des vorgegebenen Umfangs lediglich Auszüge aus den jeweiligen Publikationen vorgestellt werden.

In **Publikation I** wurde in einem standardisierten Testaufbau die Größe und Geometrie der produzierten Läsionen untersucht. In den makroskopischen Messungen der 3 cm-Läsionen erreichten alle verwendeten Systeme die Zielvorgabe vom 14,14 cm^3. Das AngioDynamics-System war mit einer Abweichung von + 21 % dem vorgegebenen Zielvolumen von 14,14 cm^3 am nächsten. Die drei anderen Systeme übertrafen das Zielvolumen mit + 101 % (Radionics) bzw. + 103 % (Celon) und + 110 % (Boston Scientific).
In den Versuchsreihen der 5 cm-Läsionen (**Publikation I**) erreichten im beschriebenen Versuchsaufbau nicht alle Geräte die Zielvorgabe von 65,45 cm^3. Während mit dem Celon-System das Zielvolumen mit +40 % weit übertroffen hat, war das Boston Scientific-System mit +10% Abweichung am nächsten am Zielvolumen. Die Systeme von Radionics- und dem AngioDynamics-System blieben mit -26 % (Radionics) und -40 % (AngioDynamics) unterhalb der Zielvorgaben.

In **Publikation II** wurden die Ergebnisse der MR-Volumetrie vorgestellt. Die Leberproben wurden vor der makroskopischen Aufarbeitung untersucht um mögliche Störeinflüsse durch die Präparation zu vermeiden. Gemittelt über alle vier RFA-Systeme und beide verwendeten Sequenzen bei den 3-cm Läsionen waren etwa 58 % des Ablationsvolumens im MRT nicht sichtbar (56,7 % in der T1 und 58,6 % in der PD-Sequenz). Die Versuchsreihen der 5 cm-Läsionen ergaben, dass gemittelt über alle vier RFA-Systeme und beide verwendeten Sequenzen circa 61 % des Ablationsvolumens im MRT nicht sichtbar waren (59,2 % in der T1 und 62,8 % in der PD-Sequenz).

Exemplarisch wurde eine Probe nach der RFA histopathologisch aufgearbeitet, um eine Zuordnung insbesondere der Außenzone der Ablation bezüglich vitalen Gewebes oder irreversibler Zelldestruktion treffen zu können (siehe **Publikation II**). In Abbildung 6 sind die makroskopisch und histologischen Veränderungen im Gewebe dargestellt.

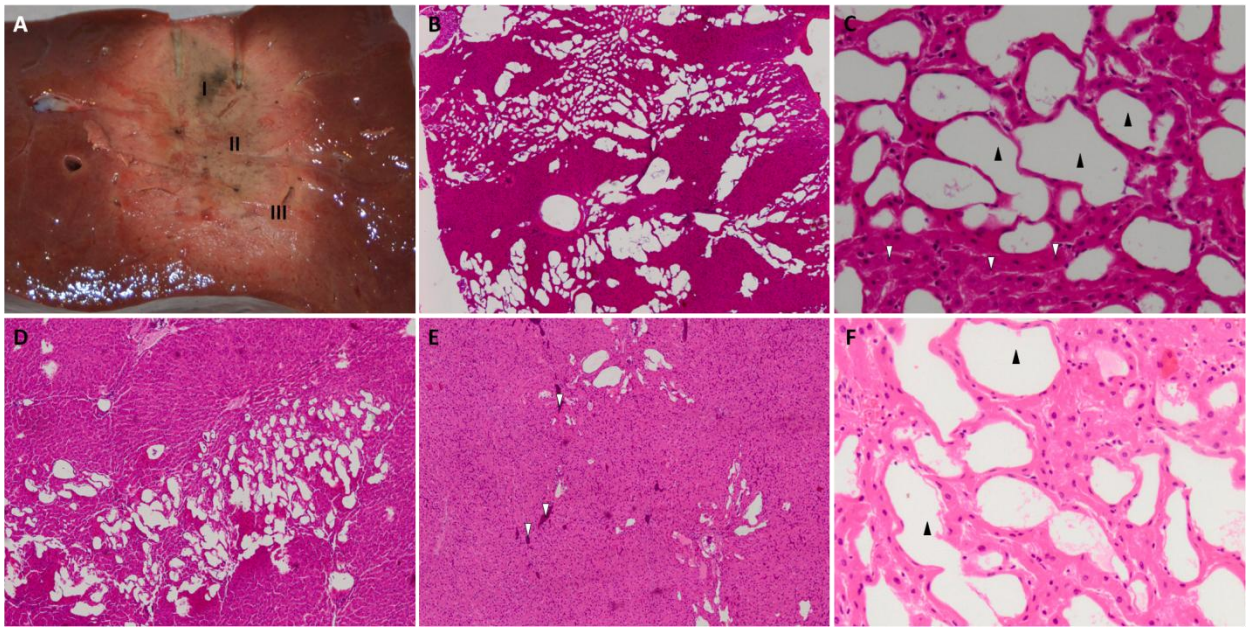

Abbildung 6 – Histopathologische Korrelation der Nekrosezonen: [A] Querschnitt einer Leberprobe nach RFA mit zwei Celon ProSurge-Elektroden. Enthalten sind die Zonen I-III (siehe Abbildung 5). [B] 40-fache Vergrößerung der Zone I mit Kauterisationsartefakten (Artefakte im Gewebe durch sehr hohe Temperaturen) entlang der Elektrode. [C] 200-fache Vergrößerung der Zone I mit pseudozystischen Zellen (= Vakuolen im Gewebe, die durch die Ausdehnung von Wasser entstanden sind (schwarze Pfeilspitzen)) und Verlust von Zellkernen (weiße Pfeilspitzen). [D] 40-fache Vergrößerung von Zone II mit partiellem Gewebestrukturverlust und pseudozystischen Zellen. [E] 40-fache Vergrößerung von Zone III mit Gerinnung innerhalb von Blutgefäßen (weiße Pfeilspitzen). [F] 200-fache Vergrößerung der Zone III mit noch vereinzelten pseudozystischen Zellen (schwarze Pfeilspitzen). [B-F] Hämatoxylin-Eosin-Färbung. Abbildung aus **Publikation II** (20).

MIKROWELLENABLATION

In **Publikation III** (22) zeigten sich mit der T1-Sequenz in den verschiedenen Versuchsreihen der MWA im MRT Volumina von 7,0 ± 1,2 cm^3 (H_2O-Injektion) bis 7,8 ± 1,3 cm^3 (12 % NaCl-Injektion). Im Vergleich dazu betrugen die Volumina in der Kontrollgruppe ohne Flüssigkeitsinjektion 7,3 ± 2,1 cm^3. Unter Verwendung der T1-Sequenz konnten keine signifikanten Unterschiede der MWA-Volumina mit Flüssigkeitsinjektion im Vergleich zur Kontrollgruppe ohne Flüssigkeitsinjektion festgestellt werden (siehe Table 3 in **Publikation III**). Unter Verwendung der PD-Sequenz zeigten sich ebenfalls keine signifikanten Unterschiede zwischen den jeweiligen Untersuchungsgruppen. Die Ergebnisse reichten von 4,9 ± 1,4 cm^3 für die Untersuchungsreihe mit 12 % NaCl bis 5,5 ± 1,9 cm^3 für die 0,9 % NaCl-Lösung. Im Vergleich dazu zeigten sich in der Kontrollgruppe ohne Flüssigkeitsinjektion Volumina von 4,7 ± 1,6 cm^3.

Ein statistisch signifikanter Unterschied ($p \leq 0,05$) wurde zwischen den beiden verwendeten Sequenzen und allen Versuchsreihen ($p < 0,001$) sowie zwischen den korrespondierenden Gruppen der verwendeten Sequenzen festgestellt (siehe Table 4 in **Publikation III**). Die Volumina, die mit der T1-Sequenz gemessen wurden, entsprachen eher dem Zielvolumen von 8 cm^3 als die mittels PD-Sequenz gemessenen Volumina.

DISKUSSION

RADIOFREQUENZABLATION

KONSTANZPRÜFUNG ZUR BERECHNUNG DES MAKROSKOPISCHEN VOLUMEN VS. MRT-VOLUMEN

Diverse Autoren haben verschiedene Verfahren zur Berechnung eines makroskopisch messbaren Volumens ausgearbeitet (21, 23). Um einen systematischen Fehler der Volumenberechnung mit der in den **Publikationen I und II** genannten Formel auszuschließen, wurden die mittels EWS-Software semiautomatisch aus den MR-Sequenzen gewonnenen Volumina mit berechneten Volumina, deren Rohdaten der x-,y- und z-Achse ebenfalls aus dem gleichen MR-Datensatz gewonnen und per Formel berechnet wurden, gegeneinander verglichen (siehe **Publikation II**). Hierbei zeigte sich eine hoch signifikante Korrelation ($p < 0,01$) mit einem Korrelationskoeffizienten von 0,888 für die T1-gewichtete Sequenz und von 0,875 für die PD-Sequenz. Den Ergebnissen zufolge kann angenommen werden, dass die verwendete Formel eine statistisch hinreichende Genauigkeit erwarten lässt und somit für weitere Versuche Verwendung finden kann.

GRÖßE UND GESTALT DER MAKROSKOPISCHEN ABLATIONSAREALE

Alle vier Systeme übertrafen das vorgegebene Zielvolumen der 3 cm-Läsionen von 14,14 cm^3. Die Systeme von Boston Scientific und Celon übertrafen ebenfalls das Zielvolumen der 5 cm-Läsionen von 65,45 cm^3. Hier sei auf die Diskussionen in **Publikation I und II** verwiesen.

Das Radionics-System blieb unter Verwendung der Cluster-Elektrode unterhalb der Zielgröße zurück. Wie bereits erwähnt, war die Cluster-Elektrode zum Zeitpunkt der Versuchsdurchführung nicht mehr für eine 5 cm-Läsion zugelassen. Die vom Hersteller zugelassene Maximalgröße betrug 4,2 x 4,5 cm für eine Einzelablation. Für größere Läsionen hätte die Elektrode repositioniert werden müssen. Da eine Repositionierung in den durchgeführten Versuchen eine unkalkulierbare Fehlerquelle bedeutet hätte, die Elektrode jedoch häufig im klinischen Alltag auch für größere Tumoren Verwendung fand, wurden die Ergebnisse für diese Elektrode unter der Vorkenntnis, dass es sich bei der 5 cm-Läsion um ein ambitioniertes Ziel handelt, in dieser Arbeit mit aufgeführt.

Das temperaturkontrollierte System von AngioDynamics blieb bei der 5 cm-Läsionsgröße signifikant unterhalb des erwarteten Zielvolumens zurück. In der Analyse der Rohdaten zeigte sich eine Spanne des x-Achsen-Querdurchmessers in den einzelnen Versuchen von 3,5 bis 6,3 cm. Somit musste von einem zufälligen Ereignis bei der geringen Fallzahl der Versuche oder

einem bisher nicht identifizierten Fehler ausgegangen werden, da in der Literatur ein solches Abweichen der Ablationsareale mit diesem System nicht beschrieben ist. Eine mögliche Störquelle in diesem Versuchsaufbau stellte die Temperatursteuerung des AngioDynamics-Systems dar. Hierbei wurde während der Ablation konstant vom System die Temperatur im Gewebe über Sensoren in den Elektrodenspitzen gemessen und bei Erreichen der Zieltemperatur die Stromzufuhr gestoppt. Da in diesem Versuchsaufbau keine Perfusion und dadurch, ähnlich des Heat-Sink-Effekts (13, 14), keine Abkühlung des Parenchyms simuliert werden konnte, ist es möglich, dass die Energiezufuhr bei konstanter Temperatur an der Elektrode zu gering war, um ein Ablationsvolumen von 65,45 cm^3 oder größer herzustellen.

Histopathologische Aufarbeitung der RFA-Läsion

In **Publikation II** wurde die histopathologische Aufarbeitung der drei Zonen nach der RFA an einer Probe aufgeführt (siehe Abbildung 6). Das histopathologische Bild der ex-vivo durchgeführten Versuche entspricht den Abbildungen und Beschreibungen aus der Arbeit von Lee. et al., welche RFA-Versuche in-vivo in Kaninchen mit einem 7-Wochen-Follow-Up durchgeführt haben (24). In dieser Studie zeigte sich in der Transitionalzone (TZ) unmittelbar nach der Intervention ebenfalls nur eine leichte Gewebsdestruktion, die jedoch nach 7 Wochen auf Grund der initialen thermischen Einwirkung nekrotisch war.

Aus diesen Ergebnissen kann die Schlussfolgerung gezogen werden, dass die makroskopische Messung die tatsächliche Ausdehnung des Nekroseareals darstellt und die Transitionalzone ebenfalls zur Gesamtnekrosezone hinzuzuzählen ist (24).

Visualisierung der Transitionalzone im MRT

Die Transitionalzone als äußerer Anteil des Ablationsareals ist im offenen MRT mit den gewählten Sequenzen nicht eindeutig beurteilbar. In vorangegangenen Studien wurde beschrieben, dass Temperaturen von etwa 50 °C über zwei Minuten zu einer irreversiblen Denaturierung der Zellen im Gewebe führten (25, 26). Dieser „Niedertemperatur"-Denaturierungseffekt entsprach in unseren Versuchen eher den Temperaturen im Randbereich der TZ als nahe an der Elektrode, wo hohe Temperaturen vorlagen und es zu einer sichtbaren Strukturveränderung bis hin zur Verkohlung des Gewebes kam (siehe Abbildung 5). Die in Zone III eher auf Zellebene stattfindenden Veränderungen waren in Summe nicht so stark ausgeprägt, als dass es direkt nach der Intervention zu einer im MRT visualisierbaren Änderung der

Protonenkonzentration beispielsweise durch Verdampfung des Gewebewassers wie in Zone I und II gekommen wäre (siehe abnehmende Zahl pseudozystischer Zellen in Abbildung 6).
Eine möglichst frühe Aussage über die Vollständigkeit der Ablation treffen zu können kann somit mit den gewählten Sequenzen nicht abschließend bzw. endgültig getroffen werden.

Makroskopische Darstellung der Transitionalzone

In der makroskopischen Messung zeigte sich, dass sich der Anteil der Transitionalzone je nach gewähltem RF-System unterschiedlich verhielt: Im Vergleich zu den 3 cm-Läsionen nahm der Anteil der TZ am Gesamtvolumen mit dem AngioDynamics- und dem Boston-Scientific-System bei der 5 cm-Läsion zu, wohingegen der Anteil der TZ mit den Systemen von Radionics und Celon abnahm.
Eine mögliche Erklärung für die Verkleinerung der TZ waren thermische Synergie-Effekte durch die Änderung der Elektrodenkonfiguration (14). Bei den Systemen von Radionics und Celon wurden im Vergleich von der 3 cm zur 5 cm-Läsion entweder unterschiedliche Elektroden verwendet (Radionics Cluster-Elektrode) oder die Anordnung der Elektroden zueinander wurde geändert (Celon-System). Beim Radionics-System wurde der aus einer Elektrode bestehende Applikator durch die Cluster-Elektrode mit drei in den Applikator integrierten Elektroden ersetzt. Beim Celon-System wurden anstatt von zwei Elektroden (3 cm-Läsionen), die in einer Linie zueinander positioniert waren, drei Elektroden (5 cm-Läsionen) in einer triangulären Position zueinander gesetzt. Diese Änderung resultiert in einem höheren Wärmeeintrag in das Gewebe und somit einem verbesserten Ablationsverhalten (27).
In der Literatur wurde bereits das Heat-trapping als Eigenschaft von bi- und multipolaren Elektroden und der daraus resultierenden, höheren Temperatur im Gewebe beschrieben (14, 28).
Diese höheren Temperaturen führten zu Veränderungen, wie sie in Zone I und II typisch sind und diese Zonen somit vergrößerten.

Mikrowellenablation

In **Publikation III** wurde der Einfluss von NaCl-Flüssigkeitsinjektionen bei der Mikrowellenablation auf das Gesamtablationsvolumen untersucht. Die verwendeten MRT-Sequenzen zeigten keine signifikanten Unterschiede zwischen den Volumina mit NaCl-Flüssigkeitsinjektion vor der Ablation im Vergleich zur Gruppe mit H_2O-Injektion sowie zur Kontrollgruppe ohne vorherige Flüssigkeitsinjektion. Somit scheint hier eine Unabhängigkeit

von normo- und hypertonen Natrium-Chlorid-Lösungen beziehungsweise zusätzlicher Wasser-Injektion zu bestehen.

Eine Erhöhung der Flüssigkeits- und/oder Natrium-Ionenkonzentration im Gewebe führte – anders als im Vergleich zur Methode der Radiofrequenzablation – nicht zu einer Vergrößerung des Ablationsareals. Die hier vorgestellten Ergebnisse sind konstant zu der in etwa zeitgleich veröffentlichten Studie von Ji et al. (29).

In den Versuchen zeigte sich eine signifikant eindeutigere Darstellung der Läsionen mit der T1-Sequenz im Vergleich zur PD-Sequenz. Diesbezüglich lässt sich jedoch feststellen, dass beide Darstellungsarten nicht zufriedenstellend sind und ein Fokus auf der Suche nach geeigneteren Sequenzen liegen sollte.

Eine Limitierung des Ablationsareals ist die mögliche Reichweite der Mikrowellen im Gewebe. Mehrere Studien haben zwischenzeitlich gezeigt, dass durch die gleichzeitige Verwendung mehrerer MW-Antennen bzw. Systeme im Gewebe auch größere Ablationsvolumina erzielt werden können als mit den Systemen der RFA (6, 30).

FAZIT

Die **Publikationen I-III** zeigten, dass mit Hilfe der RFA und der MWA insbesondere kleinere Läsionen von allen gängigen Systemen abladiert werden können. Wie in **Publikation I** aufgeführt, entsprach das produzierte Volumen selbst unter Bedingungen ohne Perfusion nur selten einer Kugel oder einem Ellipsoid. Im patientenindividuellen Behandlungskonzept ist das Wissen um die Geräteeigenschaften und das Ablationsverhalten der jeweiligen Systeme von großer Bedeutung, um einen initialen Therapieerfolg im Sinne einer vollständigen Ablation zu gewährleisten.

Die **Publikationen II und III** zeigten, dass die Visualisierung des Ablationsareals von den gewählten Sequenzen abhing und im Vergleich zum makroskopisch gemessenen Volumen die visualisierten MR-Volumina grundsätzlich kleiner waren. In unseren Versuchen konnte mit den gewählten MR-Sequenzen das abladierte Gewebe im Randbereich nur unzureichend vom gesunden Gewebe abgegrenzt werden. Der in **Publikation II** beschriebene Korrekturfaktor für MR-Volumina stellt eine Berechnungsgrundlage dar, um unter ex-vivo-Bedingungen auf das mögliche Zielvolumen schließen zu können. Jedoch lassen diese Daten nur bedingt Rückschlüsse

auf in-vivo-Therapien zu. Möglicherweise eröffnet die MR-Thermometrie, die diffusionsgewichtete MR-Bildgebung oder MR-Hybridbildgebung Wege zur eindeutigeren Beurteilung von Thermoablationsarealen. Wie die hier vorgestellten Versuche in **Publikation I und II** zeigten, stellen Läsionen von 5 cm Durchmesser erhöhte Anforderungen sowohl an den Bediener, als auch an das System, insbesondere für die akkurate Ablationsvolumenerreichung.
Wie in **Publikation III** aufgeführt, konnte unter Verwendung der Mikrowellen-Technik das Ablationsvolumen mit vorherigen Flüssigkeitsinjektionen nicht vergrößert werden. Somit muss nach aktuellem Stand mit mehreren Antennen und Systemen gearbeitet werden, um größere Tumorherde therapieren zu können. Auf Grund der Unabhängigkeit der MWA vom Flüssigkeitsanteil im Gewebe kann dieses Verfahren einen Vorteil gegenüber der RFA bei Patienten mit bindegewebigen Parenchymveränderungen wie einer Leberzirrhose haben.

LITERATURVERZEICHNIS

1. Villain P, Gonzalez P, Almonte M, Franceschi S, Dillner J, Anttila A, Park JY, De Vuyst H, Herrero R. European Code against Cancer 4th Edition: Infections and Cancer. Cancer Epidemiol. 2015;39 Suppl 1:S120-38.
2. Ferlay J, Soerjomataram I, Dikshit R, Eser S, Mathers C, Rebelo M, Parkin DM, Forman D, Bray F. Cancer incidence and mortality worldwide: sources, methods and major patterns in GLOBOCAN 2012. Int J Cancer. 2015;136(5):E359-86.
3. El-Serag HB. Epidemiology of viral hepatitis and hepatocellular carcinoma. Gastroenterology. 2012;142(6):1264-73 e1.
4. Brace CL. Radiofrequency and microwave ablation of the liver, lung, kidney, and bone: what are the differences? Curr Probl Diagn Radiol. 2009;38(3):135-43.
5. Hocquelet A, Balageas P, Laurent C, Blanc JF, Frulio N, Salut C, Cassinotto C, Saric J, Possenti L, Bernard PH, Montaudon M, Trillaud H. Radiofrequency ablation versus surgical resection for hepatocellular carcinoma within the Milan criteria: A study of 281 Western patients. Int J Hyperthermia. 2015;31(7):749-57.
6. Ryan MJ, Willatt J, Majdalany BS, Kielar AZ, Chong S, Ruma JA, Pandya A. Ablation techniques for primary and metastatic liver tumors. World J Hepatol. 2016;8(3):191-9.
7. Delis SG, Dervenis C. Selection criteria for liver resection in patients with hepatocellular carcinoma and chronic liver disease. World J Gastroenterol. 2008;14(22):3452-60.
8. Forner A, Bruix J. The size of the problem: clinical algorithms. Dig Dis. 2013;31(1):95-103.
9. Forner A, Llovet JM, Bruix J. Hepatocellular carcinoma. Lancet. 2012;379(9822):1245-55.
10. Chen L, Sun J, Yang X. Radiofrequency ablation-combined multimodel therapies for hepatocellular carcinoma: Current status. Cancer Lett. 2016;370(1):78-84.
11. Kim YS, Lee WJ, Rhim H, Lim HK, Choi D, Lee JY. The minimal ablative margin of radiofrequency ablation of hepatocellular carcinoma (> 2 and < 5 cm) needed to prevent local tumor progression: 3D quantitative assessment using CT image fusion. AJR Am J Roentgenol. 2010;195(3):758-65.
12. Lee DH, Lee JM, Lee JY, Kim SH, Han JK, Choi BI. Radiofrequency ablation for intrahepatic recurrent hepatocellular carcinoma: long-term results and prognostic factors in 168 patients with cirrhosis. Cardiovasc Intervent Radiol. 2014;37(3):705-15.
13. Mahnken AH, Bruners P, Gunther RW. Techniques of interventional tumor therapy. Dtsch Arztebl Int. 2008;105(38):646-53.
14. Brace CL, Sampson LA, Hinshaw JL, Sandhu N, Lee FT, Jr. Radiofrequency ablation: simultaneous application of multiple electrodes via switching creates larger, more confluent ablations than sequential application in a large animal model. J Vasc Interv Radiol. 2009;20(1):118-24.
15. Schwartz LH, Seymour L, Litiere S, Ford R, Gwyther S, Mandrekar S, Shankar L, Bogaerts J, Chen A, Dancey J, Hayes W, Hodi FS, Hoekstra OS, Huang EP, Lin N, Liu Y, Therasse P, Wolchok JD, de Vries E. RECIST 1.1 - Standardisation and disease-specific adaptations: Perspectives from the RECIST Working Group. Eur J Cancer. 2016;62:138-45.
16. Cabibbo G, Maida M, Genco C, Alessi N, Peralta M, Butera G, Galia M, Brancatelli G, Genova C, Raineri M, Orlando E, Attardo S, Giarratano A, Midiri M, Di Marco V, Craxi A, Camma C. Survival of patients with hepatocellular carcinoma (HCC) treated by percutaneous radio-frequency ablation (RFA) is affected by complete radiological response. PLoS One. 2013;8(7):e70016.
17. Streitparth F, Knobloch G, Balmert D, Chopra S, Rump J, Wonneberger U, Philipp C, Hamm B, Teichgraber U. Laser-induced thermotherapy (LITT)--evaluation of a miniaturised

applicator and implementation in a 1.0-T high-field open MRI applying a porcine liver model. Eur Radiol. 2010;20(11):2671-8.
18. Lee JM, Kim SH, Han JK, Sohn KL, Choi BI. Ex vivo experiment of saline-enhanced hepatic bipolar radiofrequency ablation with a perfused needle electrode: comparison with conventional monopolar and simultaneous monopolar modes. Cardiovasc Intervent Radiol. 2005;28(3):338-45.
19. Schmidt D, Trubenbach J, Konig CW, Brieger J, Duda S, Claussen CD, Pereira PL. [Radiofrequency ablation ex vivo: comparison of the efficacy of impedance control mode versus manual control mode by using an internally cooled clustered electrode]. Rofo. 2003;175(7):967-72.
20. Rathke H, Hamm B, Guettler F, Lohneis P, Stroux A, Suttmeyer B, Jonczyk M, Teichgraber U, de Bucourt M. Volume comparison of radiofrequency ablation at 3- and 5-cm target volumes for four different radiofrequency generators: MR volumetry in an open 1-T MRI system versus macroscopic measurement. Biomed Tech (Berl). 2015;60(6):521-31.
21. Rathke H, Hamm B, Guttler F, Rathke J, Rump J, Teichgraber U, de Bucourt M. Comparison of four radiofrequency ablation systems at two target volumes in an ex vivo bovine liver model. Diagn Interv Radiol. 2014;20(3):251-8.
22. Collettini F, Rathke H, Schnackenburg B, Thomas A, Albrecht L, Suttmeyer B, Jonczyk M, Guettler F, Teichgraber U, Kroncke T, Hamm B, de Bucourt M. Fluid preinjection for microwave ablation in an ex vivo bovine liver model assessed with volumetry in an open MRI system. Diagn Interv Radiol. 2013;19(5):427-32.
23. Breen MS, Lancaster TL, Lazebnik RS, Nour SG, Lewin JS, Wilson DL. Three-dimensional method for comparing in vivo interventional MR images of thermally ablated tissue with tissue response. J Magn Reson Imaging. 2003;18(1):90-102.
24. Lee JD, Lee JM, Kim SW, Kim CS, Mun WS. MR imaging-histopathologic correlation of radiofrequency thermal ablation lesion in a rabbit liver model: observation during acute and chronic stages. Korean J Radiol. 2001;2(3):151-8.
25. Veenendaal LM, Borel Rinkes IH, van Hillegersberg R. Multipolar radiofrequency ablation of large hepatic metastases of endocrine tumours. Eur J Gastroenterol Hepatol. 2006;18(1):89-92.
26. Bruners P, Schmitz-Rode T, Gunther RW, Mahnken A. Multipolar hepatic radiofrequency ablation using up to six applicators: preliminary results. Rofo. 2008;180(3):216-22.
27. Clasen S, Schmidt D, Boss A, Dietz K, Krober SM, Claussen CD, Pereira PL. Multipolar radiofrequency ablation with internally cooled electrodes: experimental study in ex vivo bovine liver with mathematic modeling. Radiology. 2006;238(3):881-90.
28. Lee JM, Han JK, Kim HC, Kim SH, Kim KW, Joo SM, Choi BI. Multiple-electrode radiofrequency ablation of in vivo porcine liver: comparative studies of consecutive monopolar, switching monopolar versus multipolar modes. Invest Radiol. 2007;42(10):676-83.
29. Ji Q, Xu Z, Liu G, Lin M, Kuang M, Lu M. Preinjected fluids do not benefit microwave ablation as those in radiofrequency ablation. Acad Radiol. 2011;18(9):1151-8.
30. Fan W, Li X, Zhang L, Jiang H, Zhang J. Comparison of microwave ablation and multipolar radiofrequency ablation in vivo using two internally cooled probes. AJR Am J Roentgenol. 2012;198(1):W46-50.

EIDESSTATTLICHE VERSICHERUNG

„Ich, Hendrik Rathke, versichere an Eides statt durch meine eigenhändige Unterschrift, dass ich die vorgelegte Dissertation mit dem Thema: „Validierung interventionell radiologischer Thermoablationsverfahren und ihre Visualisierung in der offenen 1 Tesla Magnetresonanztomographie“ selbstständig und ohne nicht offengelegte Hilfe Dritter verfasst und keine anderen als die angegebenen Quellen und Hilfsmittel genutzt habe.
Alle Stellen, die wörtlich oder dem Sinne nach auf Publikationen oder Vorträgen anderer Autoren beruhen, sind als solche in korrekter Zitierung (siehe „Uniform Requirements for Manuscripts (URM)“ des ICMJE -*www.icmje.org*) kenntlich gemacht. Die Abschnitte zu Methodik (insbesondere praktische Arbeiten, Laborbestimmungen, statistische Aufarbeitung) und Resultaten (insbesondere Abbildungen, Graphiken und Tabellen) entsprechen den URM (s.o) und werden von mir verantwortet.
Mein Anteil an der ausgewählten Publikation entspricht dem, der in der untenstehenden gemeinsamen Erklärung mit dem Betreuer, angegeben ist.

Die Bedeutung dieser eidesstattlichen Versicherung und die strafrechtlichen Folgen einer unwahren eidesstattlichen Versicherung (§156,161 des Strafgesetzbuches) sind mir bekannt und bewusst.“

_____

Datum Unterschrift

ANTEILSERKLÄRUNG AN DEN IN DIESER RAHMENSCHRIFT EINBEZOGENEN PUBLIKATIONEN

Hendrik Rathke hatte folgenden Anteil an den in diese Rahmenschrift einbezogenen Publikationen:

Publikation I

Rathke H, Hamm B, Güttler F, Rathke J, Rump J, Teichgräber U, de Bucourt M. *Comparison of four radiofrequency ablation systems at two target volumes in an ex vivo bovine liver model.* Diagn Interv Radiol. 2014 May-Jun;20(3):251-8. doi: 10.5152/dir.2013.13157. Impact Factor 1,406 (2015).

Beitrag im Einzelnen: Beteiligung an der Planung des Versuchsaufbaus und -ablaufs. Durchführung der Versuche und Datenakquisition. Auswertung und Interpretation der gewonnenen Daten. Erstellen des Manuskripts mit Einreichung beim Journal. Endgültige Zustimmung nach dem Peer-Review zur Veröffentlichung.

Publikation II

Rathke H, Hamm B, Güttler F, Lohneis P, Stroux A, Suttmeyer B, Jonczyk M, Teichgräber U, de Bucourt M. *„Volume comparison of radiofrequency ablation at 3- and 5-cm target volumes for four different radiofrequency generators: MR volumetry in an open 1-T MRI system versus macroscopic measurement.“* Biomed Tech (Berlin). 2015 Dec 1;60(6):521-31. doi: 10.1515/bmt-2014-0174. Impact Factor 1,650 (2015).

Beitrag im Einzelnen: Beteiligung an der Planung des Versuchsaufbaus und -ablaufs. Durchführung der Versuche und Datenakquisition am offenen MRT. Auswertung und Interpretation der gewonnenen Daten. Erstellen des Manuskripts mit Einreichung beim Journal. Endgültige Zustimmung nach dem Peer-Review zur Veröffentlichung.

Publikation III

Collettini F, Rathke H, Schnackenburg B, Thomas A, Albrecht L, Suttmeyer B, Jonczyk M, Guettler F, Teichgräber U, Kroncke T, Hamm B, de Bucourt M. *Fluid preinjection for microwave ablation in an ex vivo bovine liver model assessed with volumetry in an open MRI*

system. Diagn Interv Radiol. 2013 Sep-Oct;19(5):427-32. doi: 10.5152/dir.2013.12189. Impact Factor 1,406 (2015).

Beitrag im Einzelnen: Mitplanung des Versuchsaufbaus und -ablaufs. Durchführung der Versuche und Datenakquisition am offenen MRT. Endgültige Zustimmung nach dem Peer-Review zur Veröffentlichung.

Unterschrift, Datum und Stempel des betreuenden Hochschullehrers

_____

Unterschrift des Doktoranden

_____

PUBLIKATION I

Diagn Interv Radiol 2014; 20:251-258
© Turkish Society of Radiology 2014

INTERVENTIONAL RADIOLOGY
ORIGINAL ARTICLE

Comparison of four radiofrequency ablation systems at two target volumes in an *ex vivo* bovine liver model

Hendrik Rathke, Bernd Hamm, Felix Güttler, Joern Rathke, Jens Rump, Ulf Teichgräber, Maximilian de Bucourt

PURPOSE
We aimed to validate actually achieved macroscopic ablation volumes in relation to calculated target volumes using four different radiofrequency ablation (RFA) systems operated with default settings and protocols for 3 cm and 5 cm target volumes in *ex vivo* bovine liver.

MATERIALS AND METHODS
Sixty-four cuboid liver specimens were ablated with four commercially available RFA systems (Radionics Cool-tip, AngioDynamic 1500X, Boston Scientific RF 3000, Celon CelonPower LAB): 16 specimens for each system; eight for 3 cm, and eight for 5 cm. Ablation diameters were measured, volumes were calculated, and RFA times were recorded.

RESULTS
For the 3 cm target ablation volume, all tested RFA systems exceeded the mathematically calculated volume of 14.14 cm^3. For the 3 cm target ablation volume, mean ablation volume and mean ablation time for each RFA system were as follows: 28.5±6.5 cm^3, 12.0±0.0 min for Radionics Cool-tip; 17.1±4.9 cm^3, 9.36±0.63 min for AngioDynamic 1500X; 29.7±11.7 cm^3, 4.60±0.50 min for Boston Scientific RF 3000; and 28.8±7.0 cm^3, 20.85±0.86 min for Celon CelonPower LAB. For the 5 cm target ablation volume, Radionics Cool-tip (48.3±9.9 cm^3, 12.0±0.0 min) and AngioDynamic 1500X (39.4±16.2 cm^3, 19.59±1.13 min) did not reach the mathematically calculated target ablation volume (65.45 cm^3), whereas Boston Scientific RF 3000 (71.8±14.5 cm^3, 9.15±2.93 min) and Celon CelonPower LAB (93.9±28.1 cm^3, 40.21±1.78 min) exceeded it.

CONCLUSION
While all systems reached the 3 cm target ablation volume, results were variable for the 5 cm target ablation volume. Only Boston Scientific RF 3000 and Celon CelonPower LAB created volumes above the target, whereas Radionics Cool-tip and AngioDynamic 1500X remained below the target volume. For the 3 cm target ablation volume, AngioDynamic 1500X with 21% deviation was closest to the target volume. For the 5 cm target volume Boston Scientific RF 3000 with 10% deviation was closest.

From the Department of Radiology (H.R., B.H., J.Rump, M.D.B. ✉ *mdb@charite.de*), Charité-University Medicine, Berlin, Germany; the Department of Radiology (F.G., U.T.), Jena University, Jena, Germany; the Department of Material Sciences and Process Engineering (J.Rathke), University of Natural Resources and Life Sciences, Vienna, Austria.

Received 12 April 2013; revision requested 27 May 2013; revision received 27 September 2013; accepted 5 October 2013.

Published online 7 February 2014.
DOI 10.5152/dir.2013.13157

Radiofrequency ablation (RFA) is a minimally invasive technique for eliminating both primary tumors and metastases. It may be particularly useful for treating patients with inoperable lesions or contraindications to open surgery. Since its introduction, percutaneous ablation has been established as an effective and safe treatment (1, 2), especially in patients with primary and secondary malignancies of the liver (3, 4), the kidney (5, 6), the lung (7, 8), and the breast (9, 10).

As radiofrequency (RF) energy can only be deployed in a closed electrical circuit, monopolar RFA devices may require up to four neutral electrodes (grounding pads), commonly placed on the thighs. The large surface of the grounding pads (manufacturer-specific, up to 200 cm^2) is intended to prevent excessive heating at the skin level; the surface of the active part(s) of the RF electrode(s) is about 100 times smaller (manufacturer-specific, usually 1–5 cm^2) than the grounding pad surface area.

Instead of monopolar systems with grounding pads, a different technique to apply RF energy is to use bipolar or multipolar devices (3, 11, 12). In bipolar devices, both the cathode and the anode are positioned within the active tip of the electrode, separated by an insulator. The current is applied between the electrodes; no grounding pads are needed. Multipolar systems induce synergetic heat effects by using a switching algorithm between two or more electrodes to induce synergetic heat effects (3).

The volume and shape of the coagulation necrosis (due to possibly different diameter extensions in the three spatial dimensions) achievable with standard clinical RF generators (apart from the generators' monopolar, bipolar or multipolar nature) depend especially on the impact of the energy applied, probe geometry, duration of heat exposure, fluid content of the target tissue, organ perfusion, and blood vessel density (13). Additionally, in *in vivo* settings, the so-called heat-sink effect has to be taken into account. The fluid content and perfusion of the tissue and blood vessel density in the target organ have been described as the main factors dissipating heat from the target site and thereby resulting in a smaller ablation volume (6).

For hepatocellular carcinoma for example, based on commonly accepted patient selection criteria, only some patients are suited for conventional surgery, mainly because patients present with poor Child-Pugh status and/or metastases in both hepatic lobes at diagnosis. Delis and Dervenis (14) report that less than 30% of hepatocellular carcinoma patients are eligible for liver resection; thus, approximately 70% require different treatment approaches.

RFA may be regarded as the most commonly used interventional modality in clinical practice, either for sole intervention or in combination with other methods, such as transarterial chemoembolization.

In a patient, the actual volume of an induced RFA can usually not be dissected and assessed macroscopically after the procedure. Interventionalists have to rely on imaging to assess the ablation volume and geometry of the induced coagulation necrosis after ablation, and hence therapeutic success. With the different RFA systems available on the market, it is valuable to have a sound understanding of the systems' behavior, especially in terms of ablation volume and geometry the specific RFA system creates, that one intends to clinically use.

The objective of this study was to validate the measured size of actual ablation volumes in relation to mathematically calculated expected ablation volumes of four different RFA systems using default settings and protocols for 3 cm and 5 cm target ablation volumes in bovine *ex vivo* liver.

Materials and methods

Study design

The study was designed to test four different RFA systems (three monopolar and one bipolar/multipolar) in terms of their ability to consistently achieve two different target ablation volumes (3 cm and 5 cm) in bovine *ex vivo* livers. RFA volumes were created in a total of 64 cuboid liver specimens (n=16 for each generator; n=8 for 3 cm and n=8 for 5 cm). For every test series, cuboids of the same liver (previously warmed to physiological body temperature of 37°C) were used for all four generators to most accurately ensure comparable tissue conditions (including impedance). All ablations were performed according to the manufacturers' protocols and/or on the basis of personal consultation with the manufacturers (details are provided in the sections on the individual RF generators below). To ensure that the entire coagulation volume could be measured, the electrodes were placed in the center of the specimen in order to provide sufficient liver tissue for the coagulation necrosis. The samples were comfortably larger than the expected lesion size. All trials were performed without repositioning the electrodes. The liver specimens were transected and inspected after RFA. Ablation diameters were recorded and volumes calculated. Temperatures inside the ablation volume during intervention and RF times were recorded.

RFA systems

The following four RFA systems, three monopolar and one bipolar/multipolar (Fig. 1, Table 1), were used as follows:

1) Cool-Tip by Radionics/Valleylab/Covidien, Mansfield, Massachusetts, USA ;
2) 1500X RF by AngioDynamics, Latham, New York, USA ;
3) RF 3000 by Boston Scientific, Natick, Massachusetts, USA ;
4) CelonPower LAB by Celon, Teltow, Germany.

The three monopolar generators have one (Radionics), two (AngioDynamics), and four (Boston Scientific) input plugs for the grounding pads. For all monopolar devices, a current balancer provided by Boston Scientific was used to evenly distribute the current to all input plugs in order to avoid unequal resistance caused by unequal distribution of current (Fig. 2). For the bipolar Celon system, the use of the balancer was not necessary.

Cool-Tip

The Cool-Tip generator yields a maximum output of 200 W and can be operated in a multipolar mode in combination with an optional switching controller, which was not used in

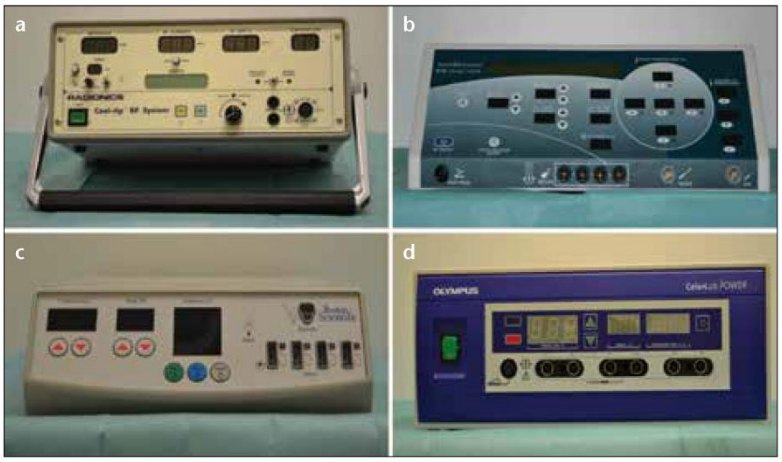

Figure 1. a–d. Photographs of the four RFA generators used. Cool-Tip by Radionics/Valleylab/Covidien **(a)**, 1500X RF by AngioDynamics **(b)**, RF 3000 by Boston Scientific **(c)**, and CelonPower LAB by Celon **(d)**.

Table 1. Overview of the four RFA systems used

	Cool-Tip	1500X RF	RF 3000	CelonPower LAB
Manufacturer	Radionics	AngioDynamics	Boston Scientific	Celon
Energy transmission	Monopolar[a]	Monopolar	Monopolar	Bi-, multipolar
Frequency	480 kHz	460 kHz	480 kHz	470 kHz
Maximum power	200 W	250 W	200 W	250 W
Applicators	1[a]	1	1	1–3
MR-compatible electrode[b]	-	+	-	+
Active tip[c]	3/2.5 cm	3/5 cm	3/5 cm	3/4 cm
Induced energy control mechanism	Impedance-controlled	Temperature-controlled	Impedance-controlled	Impedance-controlled

[a]The cluster electrode contains three electrodes in one applicator.
[b]The RF generators must under any circumstance remain outside the scanner room.
[c]For the 3/5 cm target ablation volumes, respectively.
RFA, radiofrequency ablation.

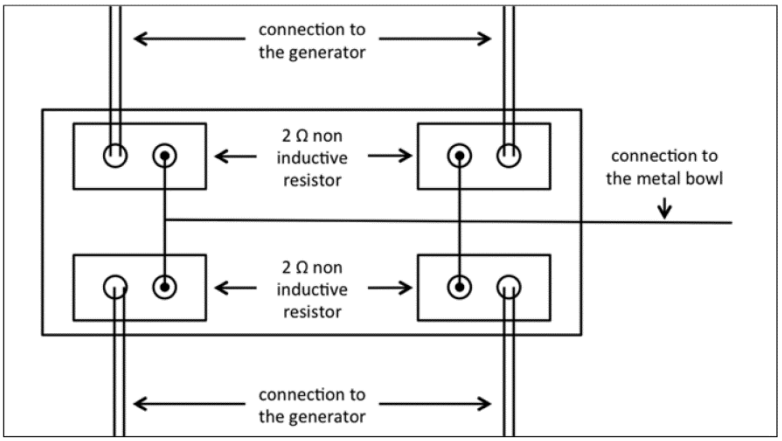

Figure 2. Schematic diagram for the mode of operation of the current balancer provided by Boston Scientific. The current balancer was used to evenly distribute the current to all input plugs, irrespective of the monopolar RF device used.

our study. The system uses an impedance-controlled algorithm. For ablation, it is important to use chilled saline in order to avoid carbonization at the electrode. Hence, the temperature at the measurable tip of the electrode should not exceed 12°C, whereas the temperature that induces coagulation necrosis in the RFA volume is, of course, much higher. If the impedance rises, the system automatically stops further delivery of energy and starts again automatically after an internally predefined decrease in impedance. For the 3 cm ablation volume, a single Cool-Tip RF electrode was used, and for the 5 cm ablation volume, the Cool-Tip cluster electrode was used. To create the latter volume, three electrodes were positioned in a prefabricated triangle with an interelectrode distance of 0.5 cm. In both cases, the ablation time was set to 12 min.

1500X RF

The monopolar generator 1500X RF has a maximum output of 250 W. Unlike the Radionics Cool-Tip, this model is temperature controlled. Every second tine of the electrode serves as a temperature probe for monitoring the inner temperature of the parenchyma during the RFA procedure. According to the protocol of AngioDynamics, a power of 150 W and a target temperature of 105°C were used for all lesions; RF time was set to 9 min to create the 3 cm ablation volume and to 15 min to create the 5 cm ablation volume. Based on the temperature-controlled mechanism, the generator only started to count off the time once the target temperature was actually reached. The RFA procedure may thus take longer than the target RF time (Tables 2 and 3). The StarBurst XL RF electrode was used for the creation of both 3 cm and 5 cm ablation volumes. This electrode can be adjusted/expanded from 2 to 5 cm. The electrode has a nine-tine Christmas tree configuration, with the option of introducing fluids, such as saline, into the tissue via an open perfusion system.

RF 3000

The impedance-controlled RF 3000 yields a maximum output of 200 W. To create a 3 cm ablation volume, according to the protocol provided, the initial output was set to 40 W and increased every 30 s by 10 W, up to a final output of 90 W. In case of an impedance increase ahead of schedule (before reaching the 90 W level, the so-called roll-off), power delivery was automatically discontinued for 30 s and started again with 50% of the roll-off power. To create a 5 cm ablation volume, according to the protocol provided, the initial output was set to 100 W and increased every 30 s by 10 W, up to a final output of 150 W. As for the 3 cm ablation volume, in case of an impedance increase ahead of schedule (before reaching the 150 W level), power delivery was automatically discontinued for 30 s and started again with 50% of the roll-off power. To create the respective ablation volumes, the umbrella-shaped twelve-tine expandable LeVeen electrode was expanded according to the manufacturer's ablation protocol to a diameter of 3 cm for the 3 cm or to a diameter of 5 cm for the 5 cm ablation volume.

CelonPower LAB

The CelonPower LAB yields a maximum output of 250 W and can be used as a bipolar and multipolar device. Up to three electrodes can be connected to one generator. The electrode contains the electric plus and minus poles at an uninsulated active tip, divided by an insulator. Hence, no dispersive pad is needed. To avoid an impedance rise, 15 current flows among the three electrodes are possible through permutations of the respective plus and minus poles. If the impedance increases between the two active tips, the generator stops power delivery to these active parts (with an automatic algorithm switching to other current pathways), preventing the use of this constellation until local impedance has decreased sufficiently. For the 3 cm lesion, two internally cooled Celon ProSurge electrodes (T30) with a 3 cm active tip were used. According to the protocol, the distance between the two electrodes was set to 1 cm. The power was set to 60 W, and the time was set to 20 min. For the 5 cm lesion, three internally cooled Celon ProSurge electrodes (T40) with a 4 cm active tip were used. According to the protocol, the distance between the three electrodes was set to 2.5 cm in an equilateral triangular configuration. In this case, the power was set to 120 W. The time was set to 40 min.

Liver specimen storage and preparation

The *ex vivo* trials were performed with fresh bovine livers provided overnight from the local slaughterhouse. A total of 16 fresh livers with peritonea were used, eight livers for the 3 cm target ablation volume and eight livers for the 5 cm target ablation volume. Approximately 10×10×8 cm or larger cuboids of the livers were prepared to ensure that the whole coagulation necrosis after RFA would easily be located inside the parenchyma. Before the specimen

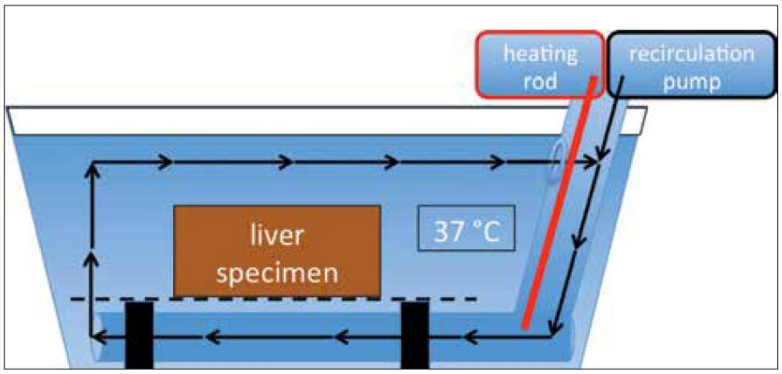

Figure 3. Diagram of 60 L water plastic tub equipped with a heating rod and recirculation pump used to warm the liver specimen to physiological body temperature of 37°C before RFA.

Figure 4. RFA setup: metal bowl filled with 0.9% saline, heated to 37°C to simulate physiological body temperature, current flow and heat conduction, cuboid liver specimen, and RF electrode *(white arrow)*. To further validate the temperature inside the parenchyma, a fiberoptic measuring system (Neoptix, Québec, Canada; *black arrow*) was positioned inside the parenchyma 1 cm from the expected center of each lesion.

preparation for RFA, all liver specimens remained in a closed cold chain of <4°C from the time of slaughter in order to prevent premature denaturation and dehydration. Before RFA, the still-sealed <4°C liver specimens were placed in a plastic tub containing 60 L of water equipped with a heating rod (Eheim Jaeger, Finsterrot, Germany) with maximum power of 200 W and a recirculation pump (Fig. 3). The temperature in the recirculating water was set to 37°C to simulate the physiological body temperature just before RFA.

After reaching physiological body temperature, the specimens were transferred into a metal bowl (filled with 37°C 0.9% saline to simulate physiological current flow and heat conduction) for RFA. The metal bowl, connected to the generators input plugs, served as the counter electrode for the current and replaced the dispersive pads used in patients. The shape of the bowl guaranteed a current flow to all sides of the specimen. For each RFA, the electrode(s) was/were maneuvered into the center of the specimen and securely fixed (Fig. 4).

Lesion size measurement

After each RFA, the specimen was cut along its electrode track. This longitudinal axis of the necrosis was defined as the x-axis. The axis perpendicular to the plane created in this way was defined as y-axis. To more accurately characterize the shape and volume of the coagulation necrosis, each created plane was again cut orthogonally to the x-y plane at the midpoint of the x-axis; the resultant cut was measured and summed to obtain the z-axis as a further measure.

Targeted spherical ablation volume is calculated as $\pi \times d^3/6$, so that targeted $V_{spherical}$=14.14 cm^3 for d=3 cm and targeted $V_{spherical}$=65.45 cm^3 for d=5 cm. Actual ablation volume is calculated as $\pi \times x \times y \times z/6$, in order to account for the possibility of ellipsoid ablation volumes.

All diameters of the ablations were measured, including the transitional zone (Fig. 5). The tissue up to the macroscopically visible hemorrhagic rim has repeatedly been postulated in the literature to correspond to a transitional zone from inner coagulation necrosis to outer normal hepatic tissue (15). Other previous studies likewise included the transitional zone of necrosis in the calculation of necrotic lesion volumes because the histopathological correlation with NADH dehydrogenase, as the vitality marker revealed irreversible cell damage at the necrotic margins and the histological assessment of *in vivo* specimens revealed irreversibly damaged cells within the hemorrhagic margins (16).

Statistical analysis

Descriptive statistical data are presented as mean±standard deviation and included data on diameters in the x-, y-, and z-axes of the RFA as well as the calculated volumes, average temperature measured 1 cm from the RFA center, and duration of RFA.

Differences in each group and between groups of the diameter measurement and volume calculation were evaluated by means of one-way analysis of vari-

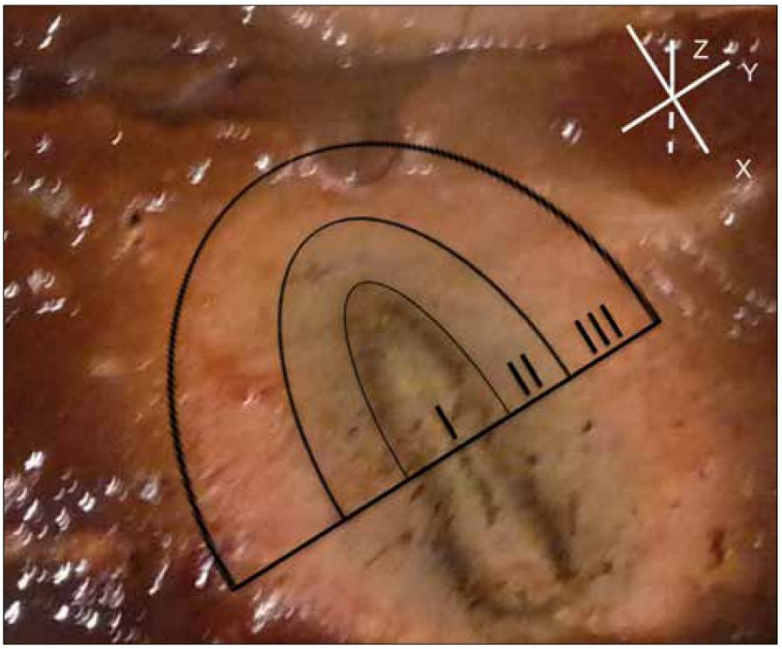

Figure 5. RFA performed under *ex vivo* conditions: (I) Necrosis/carbonization zone; (II) coagulation zone; (III) transitional zone. The upper right aspect depicts the three spatial dimensions according to the defined ablation volume alignment in the x-, y-, and z-axes. Note the central indentation of the RF electrode.

Table 2. Performance parameters of the four RFA systems for 3 cm target ablation volume

	Cool-Tip	1500X RF	RF 3000	CelonPower LAB
Manufacturer	Radionics	AngioDynamics	Boston Scientific	Celon
x-axis[a] (cm)	4.0±0.5	3.3±0.3	3.7±0.6	4.0±0.5
y-axis[b] (cm)	3.7±0.4	3.0±0.6[c]	3.8±0.7[c]	3.5±0.4
x/y quotient[d]	1.09±0.14	1.14±0.23	0.98±0.18	1.17±0.16
z-axis[e] (cm)	3.8±0.5	3.2±0.4	3.9±0.5	3.9±0.6
Volume (cm^3)	28.5±6.5	17.1±4.9[f]	29.7±11.7[f]	28.8±7.0
Ablation time[g] (min)	12.0±0.0	9.36±0.63	4.60±0.50	20.85±0.86
Temperature[g] (°C)	72.5±14.9	60.8±10.9	61.6±22.0	54.2±15.0
P[h]	< 0.001	0.135	0.007	0.001
Deviation[i] (%)	101	21	110	103

Overall P values for ANOVA are significant ($P \leq 0.043$): i.e., x-, y-, and z-axis, and volume.
[a]Diameter in the longitudinal axis along the electrode track.
[b]Diameter in the perpendicular axis in the plane created by cutting along the electrode track.
[c]$P = 0.04$ for AngioDynamics vs. Boston Scientific.
[d]Degree of sphericity: the more spherical, the more the ratio approaches 1.
[e]Diameter in the axis orthogonal to the x-y plane, at the midpoint of the x-axis on both sides, summated.
[f]$P = 0.03$ for AngioDynamics vs. Boston Scientific.
[g]Values for ablation time and temperature have descriptive character and were not used for ANOVA.
[h]Double t test for paired samples: a value $P < 0.05$ implies a significant difference between the actual and the mathematically calculated volume.
[i]Percent deviation of the actual volume from the mathematically calculated volume (14.14 cm^3).
Data are presented as mean±standard deviation for the 3 cm RF-induced coagulation necrosis.

ance (ANOVA). RFA time and temperature measurement were excluded from calculations in the analysis of variance.

For the analysis, a computer software (Statistical Package for Social Sciences, Version 19.01, SPSS Inc., Chicago, Illinois, USA) was used. To compare the test settings, ANOVA, followed by post-hoc tests with Scheffé's method, was performed. A double t-test for paired samples was performed to compare actual vs. mathematically calculated volumes Statistical level of significance was set to $P < 0.05$.

Results

The induced coagulation necroses were homogeneous and continuous for both 3 cm and 5 cm target lesion volumes and for all four generators. Sixty-four thermal ablation volumes were created in 16 livers. For each generator, 16 ablation volumes were produced (eight for 3 cm ablation volumes, and eight for 5 cm ablation volumes).

The performance parameters for the four RFA systems are presented in Table 2 for the 3 cm target ablation volume and in Table 3 for the 5 cm target ablation volume.

3 cm target ablation volume

As indicated in Table 2, all of the RFA systems exceeded 3 cm in diameter in the x-, y-, and z-axes and achieved the expected target volume for 3 cm ablation volume.

The AngioDynamics system was closest to the target volume, with a percentage deviation of 21%. The Radionics (101%), Celon (103%), and Boston Scientific (110%) systems had a greater percentage deviation from the prescribed target volume.

Considering ablation sphericity, the most spherical 3 cm lesion, as indicated by the x/y quotient, was produced with the Boston Scientific system (0.98±0.18 [reciprocal equivalent to 1.02±0.21]). The longest mean ablation diameters of each RFA system in the three spatial dimensions (dominant ablation axis) were reached along the x-axis with the single Cool-Tip electrode for the Radionics, with the nine-tine expandable electrode for the AngioDynamics, and with the Celon ProSurge electrodes for the Celon systems (4.0±0.5, 3.3±0.3, and 4.0±0.5 cm, respectively); along the z-axis as the dominant ablation axis, the twelve-tine expandable electrode for the Boston Scientific system was longest (3.9±0.5 cm). The most ellipsoid ablation volumes in the x-y plane were created by the Celon system (x/y, 1.17±0.16), followed by the

Table 3. Performance parameters of the four RFA systems for 5 cm target ablation volume

	Cool-Tip	1500X RF	RF 3000	CelonPower LAB
Manufacturer	Radionics	AngioDynamics	Boston Scientific	Celon
x-axis[a] (cm)	4.4±0.5[b]	4.5±0.6[b]	4.1±0.5[b]	5.4±0.5[b]
y-axis[c] (cm)	4.6±0.4[d]	4.2±1.0[d]	5.9±1.0[d]	5.3±0.7
Mean x/y quotient[e]	0.96±0.13	1.11±0.24	0.73±0.23	1.02±0.14
z-axis[f] (cm)	4.6±0.5[g,h]	3.9±0.5[g,h]	5.8±0.5[h]	6.1±1.1[g]
Volume (cm^3)	48.3±9.9[i]	39.4±16.2[i,j]	71.8±14.5[j]	93.9±28.1[i]
Ablation time[k] (min)	12.0±0.0	19.59±1.13	9.15±2.93	40.21±1.78
Temperature[k] (°C)	60.0±23.2	57.6±23.0	84.5±7.7	79.6±18.6
P[l]	0.002	0.003	0.25	0.024
Deviation[m] (%)	26	40	10	43

Overall *P* values for ANOVA are significant ($P \leq 0.004$): i.e., x-, y-, z-axis, x/y quotient, and volume.
[a]Diameter in the longitudinal axis along the electrode track.
[b]$P = 0.01$ for Radionics vs. Celon; $P = 0.001$ for AngioDynamics vs. Celon; $P < 0.001$ for Boston Scientific vs. Celon.
[c]Diameter in the perpendicular axis in the plane created by cutting along the electrode track.
[d]$P = 0.03$ for Radionics vs. Boston Scientific; $P = 0.003$ for AngioDynamics vs. Boston Scientific.
[e]Degree of sphericity: the more spherical, the more the ratio approaches 1.
[f]Diameter in the axis orthogonal to the x-y plane, at the midpoint of the x-axis on both sides, summated.
[g]$P = 0.002$ for Radionics vs. Celon; $P < 0.001$ for AngioDynamics vs. Celon.
[h]$P = 0.02$ for Radionics vs. Boston Scientific; $P < 0.001$ for AngioDynamics vs. Boston Scientific.
[i]$P < 0.001$ for Radionics vs. Celon; $P < 0.001$ for AngioDynamics vs. Celon.
[j]$P = 0.02$ for AngioDynamics vs. Boston Scientific.
[k]Values for ablation time and temperature measurement have descriptive character and were not used for ANOVA.
[l]Double t test for paired samples: a value $P < 0.05$ implies a significant difference between the actual and the mathematically calculated volume.
[m]Percentage deviation of the actual volume from the mathematically calculated volume (65.45 cm^3).
Data are presented as mean±standard deviation for the 5 cm RF-induced coagulation necrosis.

AngioDynamics and Radionics systems (x/y, 1.14±0.23 and 1.09±0.14).

The largest mean ablation volume was produced with the monopolar Boston Scientific system with expandable electrodes (29.7±11.7 cm^3; mean ablation time, 4.6±0.50 min), followed by the bipolar Celon (28.8±7.0 cm^3; mean ablation time, 20.85±0.86 min) and the Radionics systems (28.5±6.5 cm^3; mean ablation time, 12±0.00 min; used in monopolar mode). The smallest mean ablation volume was reached with the AngioDynamics system (17.1±4.9 cm^3; mean ablation time, 9.36±0.63 min). There was a significant difference in volume between the Boston Scientific and AngioDynamics systems ($P = 0.03$).

Accounting for the possibility of ellipsoid volumes ($V_{ellipsoid}=\pi*x*y*z/6$; with x, y, and z being the mean ablation diameters of the respective spatial axes), all of the tested RFA systems exceeded the mathematically calculated target ablation volume of 14.14 cm^3.

5 cm target ablation volume

As indicated in Table 3, only the Celon system achieved at least 5 cm diameters in the x-, y-, and z-axes. The Radionics, Boston Scientific and AngioDynamics systems did not achieve the preset diameters in all three axes.

With a percentage deviation of 10% the Boston Scientific system was closest to the set volume. The Radionics (26%) the AngioDynamics (40%), and the Celon system (43%) had greater percentage deviations from the prescribed target volume.

In terms of ablation sphericity, the most spherical 5 cm lesion, as indicated by the x/y quotient, was produced with the Celon system, using three electrodes in a triangular configuration (x/y, 1.02±0.14). The longest mean ablation diameters within each RFA system in the three spatial dimensions (dominant ablation axis) were reached along the x-axis with the expandable nine-tine electrode for the AngioDynamics system (4.5±0.6 cm), along the y-axis with the Cool-Tip cluster electrode for the Radionics system or with the 12-tine expandable electrode for the Boston Scientific system (4.6±0.4 cm; 5.9±1.0 cm), and along the z-axis with the Celon ProSurge electrodes for the Celon system (6.1±1.1 cm). The most ellipsoid ablation volumes in the x/y plane were created by the Boston Scientific system (x/y, 0.73±0.23 [reciprocal equivalent to 1.37±0.33]).

The largest mean ablation volume was produced with the Celon system (93.9±28.1 cm^3; mean ablation time, 40.21±1.78 min), followed by the Boston Scientific (71.8±14.5 cm^3; mean ablation time, 9.15±2.93 min) and the Radionics systems (48.3±9.9 cm^3; mean ablation time, 12.0±0.0 min; used in monopolar mode). The smallest mean ablation volume was reached with the AngioDynamics system (39.4±16.2 cm^3; mean ablation time, 19.59±1.13 min). There was a significant difference in the volumes between the Celon system and both the Radionics and AngioDynamics systems (each $P < 0.001$), as well as between the AngioDynamics and Boston Scientific systems ($P = 0.02$).

Accounting for the possibility of ellipsoid volumes, the Radionics system (V=48.3±9.9 cm^3) and the AngioDynamics system (V=39.4±16.2 cm^3) did not reach the mathematically calculated target ablation volume of 65.45 cm^3, whereas the Celon system (V=93.9±28.1 cm^3) and the Boston scientific system (V=71.8±14.5 cm^3) exceeded it.

Discussion

The aim of this study was to validate the agreement of mathematically calculated ablation volumes with the actual ablation volumes produced with four RFA systems using the default settings. This was achieved by evaluating how accurately the four systems tested achieved the predefined ablation diameters of 3 cm and 5 cm and the associated volumes of 14.14 and 65.45 cm^3. Mathematical volumes of 3 cm and 5 cm were tested to challenge the four RFA systems with a common lesion size, as well as with the maximum comparable lesion sizes.

Achieving an adequate predefined ablation volume may be regarded as an important prerequisite for the safe and successful RFA of a tumor. It is therefore essential to most accurately obtain this desired ablation volume without overly exceeding it (and thereby possibly damaging too much healthy tissue or important nearby structures),

as well as to be able to reproduce the results with little variability.

Having a sound understanding, not only of the three-dimensional shape but also of the orientation of the (possibly ellipsoid) ablation volume to be induced by the RF device inside the organ is crucial for preventing tumor progression and achieving therapeutic success. In a 5 cm target ablation volume, for instance, it is crucial to be aware that the 12-tine expandable electrode of the Boston Scientific system creates its longest ablation diameter along the y-axis, whereas the ablation diameter along the x-axis is considerably shorter.

For all RFA systems, a homogeneous and continuous target ablation volume with 3 cm in diameter (equivalent to 14.14 cm^3) was comfortably achieved. A rather spherical ablation zone was observed with the Boston Scientific system. The other three devices created more ellipsoid ablation volumes.

For the 3 cm ablation, the AngioDynamics system was closest to the mathematically calculated volume, with a deviation of 21% (actual volume of 17.1 cm^3 in comparison to the mathematically calculated volume of 14.14 cm^3). The other three systems deviated from the target volume by over 100%: Radionics, 101% (actual volume, 28.5 cm^3), Celon, 103% (28.8 cm^3), and Boston Scientific, 110% (29.7 cm^3).

In contrast, the 5 cm diameter target ablation volume (equivalent to 65.45 cm^3) was still comfortably exceeded with the Celon system and the Boston Scientific system, whereas the Radionics and the AngioDynamics systems failed to achieve the target volume.

In this regard, several factors have to be taken into account. The CoolTip cluster electrode for the Radionics system recently received a modified approval for ablations of up to 4.2×4.5 cm in diameter (tested by the manufacturer in 20°C bovine livers without repositioning of the electrode; manufacturer's data). For larger target ablation volumes, the use of a switching controller in combination with the RF generator and three separate monopolar electrodes is recommended. An alternative option is to reposition the electrode after the first ablation to expand the target volume.

To obtain an impression of which maximum diameters and volumes the Radionics system in combination with the cluster electrode is able to create in our standardized test set-up, the trials were performed without switching the controllers.

With the temperature-controlled AngioDynamics system, the achieved ablation diameters for the 5 cm target ablation volume ranged from 3.5 to 6.3 cm. In this RF series, the first two and again the last two ablation diameters exceeded 5 cm. We assumed that this is a coincidence or an unidentified malfunction of the generator, as no other explanation is apparent for this variation.

The large target ablation volume achieved with the Celon system (93.9±28.1 cm^3) may be favored by the long ablation time of 40 min in comparison to 20, 12, and 9 min for the other generators (AngioDynamics, Radionics, Boston Scientific, respectively). The long ablation time has the potential to smoothen and to more consistently secure a higher energy deposit in the parenchyma. In any case, the tendency to create large volumes with this RFA system in 5 cm target diameter ablations should be taken into account in order to most accurately obtain the desired ablation volume without exceeding. With the 12-tine monopolar LeVeen electrode of the Boston Scientific system, the ablation volume (71.8±14.5 cm^3) was still above the target volume of 65.45 cm^3. For the 5 cm target volume, the Boston Scientific system created a doughnut-like outer ablation shape (no central area of sparing inside the produced lesion). The Radionics system created a spherical coagulation, while the AngioDynamics and Celon systems created ellipsoid coagulations. One factor contributing to the dimensions of the produced ablation volumes may also be heat trapping between the electrodes (17, 18).

For the 5 cm ablation, the Boston Scientific system, with a 10% deviation and an actual volume of 71.8 cm^3, was closest to the mathematically calculated volume of 65.45 cm^3. The Radionics system (26%, 48.3 cm^3) and the AngioDynamics system (40%, 39.4 cm^3) remained below the target volume. The Celon system created a volume 93.9 cm^3, corresponding to a 43% deviation from the target volume.

Increased vascularization, large vessels in the vicinity (heat sink effect), or changes in the parenchymal consistency (e.g., cirrhosis or chemotherapy) may have different effects on the ablation volumes achieved in patients that were not accounted for in this *ex vivo* study design. Additionally, the ablations were performed in disease- and tumor-free parenchyma, which may render different volumes compared to the RFA of a lesion.

A comparison of the energy deposited in the tissue by the four generators investigated was not possible, as the Celon and the AngioDynamics systems do, but the Radionics and Boston Scientific systems do not, feature the required software. Calculating the electricity consumption was not considered appropriate, as the generators (as well as possible supplements such as saline pumps) require different amounts of power, precluding a straightforward comparison of the energy delivered to the tissue from an electricity consumption approach.

A possible limitation of the RF technique in general, concerning its heat conduction in a clinical setting, is the heat-mediated dehydration of a tissue, which is followed by carbonization and an increase in impedance that may reduce the RF output into the target volume.

The wide range of achieved ablation diameters and volumes (Tables 2, 3) and the standard deviations for each of the four devices, despite the highly controlled environment, requires some explanation. In an *ex vivo* setting, a consistent ablation volume is only achieved if the tissue conditions are identical, especially if the impedance remains constant. Small differences in hydration or tissue properties (e.g., fatty liver, animal age) are sufficient to cause differences in impedance and hence to result in deviations from the target diameter and volume. In the devices used in our study, a marked rise in impedance shuts down the power supply to avert the carbonization caused by the dehydration of the surrounding tissue (11). This power fluctuation may result in lower or higher ablation volumes, explaining the wide range of volumes measured.

In vivo studies have shown that the RFA volumes achieved in cirrhotic livers or after chemotherapy may vary due to changes in the liver impedance (19). Therefore, the assessment of ablation-induced tissue lesions by validated imaging techniques is essential.

However, although the experiments were conducted under near physiological conditions, the heat sink effect, a main cause of inadequate ablation (3), was absent in our experimental setup. Therefore, a larger necrosis volume should not necessarily be considered a disadvantage of each respective system; rather, this may provide the reserve necessary to compensate for a high vessel density in tumor tissues.

When using one of the tested RFA systems, it is important to keep in mind that our results are *ex vivo* results and may differ from ablation diameters *in vivo*.

In conclusion, it is neither intended nor possible to make a straightforward recommendation in favor of one of the RFA systems tested in this study. The RFA systems available on the market differ. Interventionalists need to keep this in mind and gain a sound understanding, especially of the ablation volume and geometry of their specific RFA system in order to achieve therapeutic success. Other factors must also be taken into account, ranging from the patient group to be treated (tumor entity, location, configuration, volume, shape, and disease progression) to the integration into a hospital's workflow (subjective ease of handling, acceptance by other staff working with the RFA system in daily clinical routine, RF time, and economic efficiency).

Conflict of interest disclosure

The authors declared no conflicts of interest.

References

1. Tacke J. Percutaneous radiofrequency ablation-clinical indications and results. Rofo 2003; 175:156–168. [CrossRef]
2. Gazelle GS, Goldberg SN, Solbiati L, Livraghi T. Tumor ablation with radiofrequency energy. Radiology 2000; 217:633–646. [CrossRef]
3. Brace CL, Sampson LA, Hinshaw JL, Sandhu N, Lee FT Jr. Radiofrequency ablation: simultaneous application of multiple electrodes via switching creates larger, more confluent ablations than sequential application in a large animal model. J Vasc Interv Radiol 2009; 20:118–124. [CrossRef]
4. Lee DH, Lee JM, Lee JY, Kim SH, Han JK, Choi BI. Radiofrequency ablation for intrahepatic recurrent hepatocellular carcinoma: long-term results and prognostic factors in 168 patients with cirrhosis. Cardiovasc Intervent Radiol 2013 Aug 3. [Epub ahead of print] [CrossRef]
5. Tacke J, Mahnken AH, Gunther RW. Percutaneous thermal ablation of renal neoplasms. Rofo 2005; 177:1631–1640. [CrossRef]
6. Mahnken AH, Rohde D, Brkovic D, Gunther RW, Tacke JA. Percutaneous radiofrequency ablation of renal cell carcinoma: preliminary results. Acta Radiol 2005; 46:208–214. [CrossRef]
7. Lee H, Jin GY, Han YM, et al. Comparison of survival rate in primary non-small-cell lung cancer among elderly patients treated with radiofrequency ablation, surgery, or chemotherapy. Cardiovasc Intervent Radiol 2012; 35:343–350. [CrossRef]
8. Kim SR, Han HJ, Park SJ, et al. Comparison between surgery and radiofrequency ablation for stage I non-small cell lung cancer. Eur J Radiol 2012; 81:395–399. [CrossRef]
9. Ohtani S, Kochi M, Ito M, et al. Radiofrequency ablation of early breast cancer followed by delayed surgical resection--a promising alternative to breast-conserving surgery. Breast 2011; 20:431–436. [CrossRef]
10. Meloni MF, Andreano A, Laeseke PF, Livraghi T, Sironi S, Lee FT Jr. Breast cancer liver metastases: US-guided percutaneous radiofrequency ablation--intermediate and long-term survival rates. Radiology 2009; 253:861–869. [CrossRef]
11. Clasen S, Rempp H, Schmidt D, et al. Multipolar radiofrequency ablation using internally cooled electrodes in ex vivo bovine liver: correlation between volume of coagulation and amount of applied energy. Eur J Radiol 2012; 81:111–113. [CrossRef]
12. Bruners P, Schmitz-Rode T, Gunther RW, Mahnken A. Multipolar hepatic radiofrequency ablation using up to six applicators: preliminary results. Rofo 2008; 180:216–222. [CrossRef]
13. Desinger K, Stein T, Tschepe J. Investigations on radiofrequency current application in bipolar technique for interstitial thermotherapy (RF-ITT). Minimal Invasive Medizin 1996; 7:92–97.
14. Delis SG, Dervenis C. Selection criteria for liver resection in patients with hepatocellular carcinoma and chronic liver disease. World J Gastroenterol 2008; 14:3452–3460. [CrossRef]
15. Lee JD, Lee JM, Kim SW, Kim CS, Mun WS. MR imaging-histopathologic correlation of radiofrequency thermal ablation lesion in a rabbit liver model: observation during acute and chronic stages. Korean J Radiol 2001; 2:151–158. [CrossRef]
16. Streitparth F, Knobloch G, Balmert D, et al. Laser-induced thermotherapy (LITT)--evaluation of a miniaturised applicator and implementation in a 1.0-T high-field open MRI applying a porcine liver model. Eur Radiol 2010; 20:2671–2678. [CrossRef]
17. Frericks BB, Ritz JP, Roggan A, Wolf KJ, Albrecht T. Multipolar radiofrequency ablation of hepatic tumors: initial experience. Radiology 2005; 237:1056–1062. [CrossRef]
18. Pereira PL, Trubenbach J, Schenk M, et al. Radiofrequency ablation: in vivo comparison of four commercially available devices in pig livers. Radiology 2004; 232:482–490. [CrossRef]
19. Glaiberman CB, Pilgram TK, Brown DB. Patient factors affecting thermal lesion size with an impedance-based radiofrequency ablation system. J Vasc Interv Radiol 2005; 16:1341–1348. [CrossRef]

PUBLIKATION II **DOI: 10.1515/BMT-2014-0174. Die Verlagsveröffentlichung ist verfügbar unter www.degruyter.com.**

DE GRUYTER Biomed. Eng.-Biomed. Tech. 2015; 60(6): 521–531

Hendrik Rathke, Bernd Hamm, Felix Guettler, Philipp Lohneis, Andrea Stroux, Britta Suttmeyer, Martin Jonczyk, Ulf Teichgräber and Maximilian de Bucourt*

Volume comparison of radiofrequency ablation at 3- and 5-cm target volumes for four different radiofrequency generators: MR volumetry in an open 1-T MRI system versus macroscopic measurement

DOI 10.1515/bmt-2014-0174
Received November 26, 2014; accepted May 7, 2015; online first June 9, 2015

Abstract

Introduction: In a patient, it is usually not macroscopically possible to estimate the non-viable volume induced by radiofrequency ablation (RFA) after the procedure. The purpose of this study was to use an *ex vivo* bovine liver model to perform magnetic resonance (MR) volumetry of the visible tissue signal change induced by RFA and to correlate the MR measurement with the actual macroscopic volume measured in the dissected specimens.

Materials and methods: Sixty-four liver specimens cut from 16 bovine livers were ablated under constant simulated, close physiological conditions with target volumes set to 14.14 ml (3-cm lesion) and 65.45 ml (5-cm lesion). Four commercially available radiofrequency (RF) systems were tested (n=16 for each system; n=8 for 3 cm and n=8 for 5 cm). A T1-weighted turbo spin echo (TSE) sequence with inversion recovery and a proton-density (PD)-weighted TSE sequence were acquired in a 1.0-T open magnetic resonance imaging (MRI) system. After manual dissection, actual macroscopic ablation diameters were measured and volumes calculated. MR volumetry was performed using a semiautomatic software tool. To validate the correctness and feasibility of the volume formula in macroscopic measurements, MR multiplanar reformation diameter measurements with subsequent volume calculation and semiautomatic MR volumes were correlated.

Results: Semiautomatic MR volumetry yielded smaller volumes than manual measurement after dissection, irrespective of RF system used, target lesion size, and MR sequence. For the 3-cm lesion, only 43.3% (T1) and 41.5% (PD) of the entire necrosis are detectable. For the 5-cm lesion, only 40.8% (T1) and 37.2% (PD) are visualized in MRI directly after intervention. The correlation between semiautomatic MR volumes and calculated MR volumes was 0.888 for the T1-weighted sequence and 0.875 for the PD sequence.

Conclusion: After correlation of semiautomatic MR volumes and calculated MR volumes, it seems reasonable to use the respective volume formula for macroscopic volume calculation. Hyperacute MRI after *ex vivo* intervention may result in the underestimation of the real expansion of the produced necrosis zone. This must be kept in mind when using MRI for validating ablation success directly after RFA. One reason for the discrepancy between macroscopic and MRI appearance immediately after RFA may be that the transitional zone shows no or only partially visible MR signal change.

Keywords: interventional radiology; liver; magnetic resonance (MR) volumetry; open magnetic resonance imaging (MRI); radiofrequency ablation.

***Corresponding author: PD Dr. med. Maximilian de Bucourt,** Dipl. Vw., Charité – University Medicine, Charitéplatz 1, 10117 Berlin, Germany, Phone: +49 30 450 627 085, Fax: +49 30 450 527 911, E-mail: mdb@charite.de

Hendrik Rathke, Bernd Hamm, Britta Suttmeyer and Martin Jonczyk: Department of Radiology, Charité – University Medicine, Charitéplatz 1, 10117 Berlin, Germany

Felix Guettler and Ulf Teichgräber: Department of Radiology, Jena University, Erlanger Allee 101, 07747 Jena, Germany

Philipp Lohneis: Department of Pathology, Charité – University Medicine, Charitéplatz 1, 10117 Berlin, Germany

Andrea Stroux: Department of Biometry and Clinical Epidemiology, Charité – University Medicine, Campus Benjamin Franklin, Hindenburgdamm 30, 12203 Berlin, Germany

Introduction

Several studies have shown radiofrequency ablation (RFA) to be a safe and reliable interventional procedure for treating both primary and secondary malignancies [16]. Liver neoplasms are common, and hepatocellular carcinoma (HCC) is among the six most common neoplasms, with an age-adjusted worldwide incidence of 16 cases per 100,000 inhabitants [7]. HCC has poor prognosis and is the third leading cause of cancer-related mortality, accounting for about 600,000 deaths annually [23, 31]. Therefore, RFA has evolved into a first-line treatment option for HCC under certain conditions [9].

According to the Barcelona Clinic Liver Cancer (BCLC) classification, only 20–30% of patients with HCC are considered for liver resection and transplantation [6] due to various patient-related factors such as performance status and Child-Pugh class, disease stage, and size and distribution of liver lesions [9]. The BCLC HCC staging and treatment guidelines recommend RFA for early stage A cancer in patients with either a single nodule ≤5 cm or three or fewer nodules ≤3 cm who have Child A-B liver disease and comorbidity, e.g., portal hypertension, splenomegaly, or abnormal bilirubin levels. For very early stage 0 HCC patients, RFA can be regarded as equivalent to liver resection [10]. Interventional procedures aim at complete tumor ablation while preserving healthy liver tissue. Kim et al. [12] recommend a minimum safety margin of 0.3 cm around the actual tumor to reduce local tumor progression.

The outcome of RFA can be evaluated by comparing the imaging appearance before and after ablation. Imaging modalities such as computed tomography (CT), magnetic resonance imaging (MRI), and ultrasound (US) have been used for this purpose [15, 27].

The ablative margin at the transition from ablated tissue to healthy parenchyma is conventionally assessed by comparing CT or MR images obtained before and after intervention [13]. Several investigators have pointed out that the primary tumor is often surrounded by microsatellite nodules, which have to be eliminated as well to ensure successful outcome [13, 22]. In clinical routine, it is not possible to dissect and inspect the liver for histological confirmation of complete tumor ablation. Instead, imaging procedures are used to assess the ablative margin and volume by comparing tumor size and shape with the ablated volume. For the evaluation of the ablative margin, MRI has been shown to be more sensitive for evaluating the ablative margin in the early period after ablation [1, 2, 28].

We conducted an experimental study comparing four different RFA generators at two different preset volumes in an open MRI system. As in real patients, it is not possible to evaluate the real macroscopic extent of the ablation volume after the procedure, and the aim of this study was to evaluate the feasibility of MR volumetry directly after RFA and to assess its capability of defining the dimensions of the necrosis produced by RFA in comparison to the actual macroscopically dissected specimen. Second, as the RFA-induced necrosis consists of three distinct zones, we aimed to evaluate whether the outer necrosis zone is detectable by MRI as well and whether there are differences with respect to lesion size and the generator type used for RFA.

Materials and methods

Procedure

Four different RFA systems (three monopolar and one bipolar/multipolar electrode) were used to create ablation diameters of 3 and 5 cm in *ex vivo* bovine liver. A total of 64 liver specimens cut from 16 livers were used to perform 16 ablations with each of the four RFA generators (3-cm lesion, n=8; 5-cm lesion, n=8). To ensure identical baseline conditions (e.g., impedance, tissue moisture), cuboids cut from the same liver were tested with all four generators. All specimens were heated to the physiological body temperature of 37°C. A detailed description of the experimental setup, generators including respective specifications, and ablation protocols used has recently been published [25].

After ablation, the liver specimens were examined by MRI in an open 1.0-T system (Philips Panorama 1.0T, Philips Medical Systems, Best, the Netherlands) using an inversion-recovery T1-weighted and a proton-density (PD)-weighted sequence (see Table 1 for details). After MRI, the specimen was transected and inspected. Lesion diameters were measured and volumes calculated. MR volumetry was performed using a software tool provided by the manufacturer [Extended MR WorkSpace 2.6.3.2 (2009) (hardware: Dell, Round Rock, TX, USA; software: Philips Medical Systems, Best, the Netherlands)].

Radiofrequency (RF) systems

For all monopolar devices, a current balancer was used to equally distribute energy to the grounding pad input plugs, thereby avoiding increased resistance due to unequal distribution of current. This system was not in use for the bipolar generator.

Radionics Cool Tip (Cool Tip; Covidien, Mansfield, MA, USA): The Cool Tip RF electrode was used for the 3-cm-target ablation. For the 5-cm ablation, the customary Cool Tip cluster electrode was used. In both cases, the ablation time was set to 12 min, and the internally cooled electrodes were cooled by 4°C NaCl fluid.

Note that the Radionics/Valleylab cluster electrode used to be approved for ablation of lesions up to 5 cm without the need for repositioning. It is now marketed for ablating lesions up to 4.2 cm. However, because of its frequent use in clinical routine and to ensure comparability to the other devices tested, it was included to assess the capability to create a 5-cm-ablation volume as well.

Table 1: MR sequence parameters.

	TR (ms)	TE (ms)	TI (ms)	FOV			Voxel size		Flip angle	Slice thickness (mm)	Slice gap (mm)
				RL (mm)	AP (mm)	FH (mm)	RL (mm)	FH (mm)			
T1 TSE IR[a]	800	12	50	118	51	200	0.6	0.5	–	4	-3
PD TSE[b]	1800	30	–	148.9	31	230	0.8	0.6	90	3	-2

[a]Inversion-prepared T1-weighted TSE sequence.

[b]Pseudo-PD-weighted TSE sequence.

PD, proton-density-weighted; TSE, turbo spin echo; IR, inversion repeat; TR, repetition time; TE, echo time; TI, inversion time; FOV, field of view; RL, right-left; AP, anterior-posterior; FH, feet-head.

1500X RF by AngioDynamics (1500X RF; AngioDynamics, Latham, NY, USA): For this generator, the StarBurst XL RF electrode was used for both the 3- and the 5-cm target ablation. This electrode has a 9-tine Christmas tree-shape configuration and can be expanded from 2 to 5 cm for adjustment to the target lesion during the intervention according to the manufacturer's protocol. This generator type features temperature-controlled current delivery to the electrode. After reaching a preset temperature level, the current delivery stops by manufacturer default.

The preset ablation times were 9 min for the 3-cm lesion and 15 min for the 5-cm lesion. Different time values in Tables 2 and 3 occurred because of the time delay due to heating up from 37°C to the preset temperature of 105°C for both lesion sizes. The ablation time started when the preset temperature inside the parenchyma was reached.

RF 3000 by Boston Scientific (RF 3000; Boston Scientific, Marlborough, MA, USA): For this generator, an umbrella-like 12-tine expandable electrode (LeVeen) was used and expanded to its 3-cm setting for 3-cm ablation and to its 5-cm maximum for the 5-cm target lesion.

According to the manufacturer's protocol, for a 3-cm lesion size, the initial power output was set to 40 W and incremented in steps of 10 W after every 30 s until the final output of 90 W was reached. For the 5-cm target ablation, the initial output was set to 100 W and increased in identical steps until maximum output of 150 W was reached.

In case of an early increase in resistance (so-called roll-off by the manufacturer), energy delivery was paused for 30 s and the procedure started again at half the energy output reached before the roll-off, according to the manufacturer's protocol.

Table 2: Three-centimeter target ablation volume: results.

	Radionics Cool Tip	AngioDynamics model 1500X	Boston Scientific RF 3000	Celon CelonPower LAB
Macroscopic measurement and calculation				
Mean ablation time (min)	12±0.00	9.36±0.63	4.6±0.50	20.85±0.86
Volume including TZ (ml)	28.2±6.5	17.1±4.9	29.7±11.7	28.7±7.0
Volume excluding TZ (ml)	9.8±3.7	5.5±3.5	13.1±12.2	9.7±3.6
Volume of the TZ (ml)	18.4±2.1	11.6±1.0	16.6±0.3	19.1±2.4
Percentage portion[a]	65.2	67.8	55.9	66.6
T1 IR sequence				
MR volume (ml)	15.2±2.3	6.3±2.3	12.9±6.5	11.3±5.2
Percentage deviation T1 vs. volume including TZ (%)[b,c]	46.0	63.4	56.8	60.6
Correction factor	1.85	2.73	2.31	2.54
PD TSE sequence				
MR volume (ml)	13.4±3.0	6.1±1.6	11.5±6.0	12.8±2.7
Percentage deviation PD TSE vs. volume including TZ (%)[c,d]	52.4	64.5	61.4	55.5
Correction factor	2.10	2.82	2.59	2.25

Data are presented as mean±SD for the 3-cm RF-induced coagulation necrosis. Correlation of MR volumes using T1 sequence vs. volumes including TZ, 0.592 ($p<0.01$), T1 sequence vs. volumes excluding TZ, 0.548 ($p<0.01$), PD sequence vs. volumes including TZ, 0.621 ($p<0.01$), and PD sequence vs. volumes excluding TZ, 0.519 ($p<0.01$). Statistically significant differences were detected for the volume including TZ vs. MR volume: T1, $p<0.01$; PD, $p<0.01$. No significant differences were detected for the volume excluding TZ vs. MR volume: T1, $p=0.076$; PD, $p=0.069$. The difference between volume including TZ vs. volume excluding TZ was significant, $p<0.001$. TZ, transitional zone; PD, proton-density-weighted; TSE, turbo spin echo; IR, inversion repeat.

[a]Portion of the TZ in relation to the entire necrosis volume.

[b]The value of the percentage deviation implies the non-visible amount of the necrosis in MRI. The visible part results by calculating 100%-(percentage deviation).

[c]Average value, 56.7%.

[d]Average value, 58.6%.

Table 3: Five-centimeter target ablation volume: results.

	Radionics Cool Tip	AngioDynamics model 1500X	Boston Scientific RF 3000	Celon CelonPower LAB
Macroscopic measurement and calculation				
Mean ablation time (min)	12±0.00	19.59±1.13	9.15±2.93	40.21±1.78
Volume including TZ (ml)	48.3±9.9	39.3±16.1	71.8±14.5	93.9±28.1
Volume excluding TZ (ml)	19.3±7.5	11.5±6.9	26.6±8.4	42.7±24.5
Volume of the TZ (ml)	28.9±1.7	27.8±6.6	45.2±4.3	51.2±2.6
Percentage portion[a]	59.8	70.1	63.0	54.5
T1 IR sequence				
MR volume (ml)	16.4±3.4	16.7±6.2	29.6±6.9	42.6±20.4
Percentage deviation T1 vs. volume including TZ (%)[b,c]	66.0	57.4	58.8	54.6
Correction factor	2.94	2.35	2.43	2.20
PD TSE sequence				
MR volume (ml)	15.6±3.6	15.2±6.3	27.4±7.2	37.5±15.0
Percentage deviation PD vs. volume including TZ (%)[c,d]	67.7	61.5	61.8	60.1
Correction factor	3.09	2.59	2.62	2.51

Data are presented as mean±SD for the 5-cm RF-induced coagulation necrosis. Correlation of MR volumes using T1 sequence vs. volumes including TZ, 0.903 ($p<0.01$), T1 sequence vs. volumes excluding TZ, 0.706 ($p<0.01$), PD sequence vs. volumes including TZ, 0.893 ($p<0.01$), and PD sequence vs. volumes excluding TZ, 0.744 ($p<0.01$). Statistically significant differences were detected for the volume including TZ vs. MR volume: T1, $p<0.01$; PD, $p<0.01$. No significant differences were detected for the volume excluding TZ vs. MR volume: T1, $p=0.102$; PD, $p=0.905$. The difference between volume including TZ vs. volume excluding TZ was significant, $p<0.001$. TZ, transitional zone; PD, proton-density-weighted; TSE, turbo spin echo; IR, inversion repeat.

[a]Portion of the TZ in relation to the entire necrosis volume.

[b]The value of the percentage deviation implies the non-visible amount of the necrosis in MRI. The visible part results by calculating 100%-(percentage deviation).

[c]Average value, 59.2%.

[d]Average value, 62.8%.

Celon Power Lab (Celon; Olympus, Shinjuku, Tokyo, Japan): With the Celon generator, up to three electrodes were connected to create a specific ablation volume. Two internally cooled electrodes (Celon ProSurge T30) with a 3-cm active tip placed in a line with an inter-electrode distance of 1 cm were used for the 3-cm lesion. The maximum preset power output for this system was 60 W for 20 min.

For the 5-cm lesion, three internally cooled electrodes (Celon ProSurge T40) with a 4-cm active tip were used. According to the manufacturer's protocol, the electrodes were positioned in a triangle configuration with an inter-electrode distance of 2.5 cm. A template provided by the manufacturer was used to keep the exact distance. The maximum power output was set to 120 W for 40 min.

Experimental procedure

Bovine liver specimens with a size of approximately 10×10×10 cm were prepared to ensure that the resulting ablation lesions were completely surrounded by liver parenchyma plus a margin to all sides even for the larger ablation volumes and inhomogeneous ablation shapes.

The specimens were stored at a temperature below 4°C until warmed to physiological body temperature to avoid premature denaturation and dehydration of the parenchyma before the test series.

For the test series, the specimens were first slowly heated to 37°C in a water tub and then transferred into a bowl filled with 0.9% saline to ensure physiological current flow and heat conduction. The grounding pad cables were connected to the metal bowl, which served as surface for the grounding pads.

The electrode(s) were placed in the center of the specimen, taking care that the active tip or the tines of specially configured electrodes were in the center of the specimen to create an ablation zone completely surrounded by tissue [25].

Histopathological examination was performed exemplarily in one randomly selected case after ablation and dissection.

Sequences, MR protocol, and MR volumetry

After ablation, the specimen was scanned in an open 1.0-T MRI system. The MR pulse sequence parameters are summarized in Table 1.

Two sequences were tested. First, a T1-weighted turbo spin echo (TSE) echo sequence with an inversion recovery (IR) was used. IR was selected to invert the contrast of long and short T1 signals; thus, long T1 signals appeared bright. Second, an improved PD-weighted TSE sequence was used. Both sequences were adjusted for bovine liver tissue, i.e., diffusion weighted imaging sequences as well as contrast agents were not performed in this *ex vivo* study.

Images were assessed with the Extended WorkSpace for a volumetric calculation, using the Extended MR WorkSpace

software version 2.6.3.2 (2009). With this system, it was possible to evaluate the dimension, shape, and volume of the resulting ablation lesion on multiplanar reformations (MPRs) and volumetric evaluation using a semiautomatic software tool (MR Systems Panorama HFO Release 2.6.5.0 2009-09-30; Philips Medical Systems, Best, the Netherlands).

To validate the correctness of the volume calculated by the semiautomatic software, diameters of the lesion identified by MRI were additionally measured virtually with the software using the same formula as for manual macroscopic measurement (formula explained in the Calculation section). Semiautomatic MR volume measurement and volume calculation by MR MPR diameter measurement were correlated. MR diameter measurement and subsequent volume calculation was only used for validation purposes; all other calculations were performed with the semiautomatically detected volumes. Figure 1 illustrate how MR volumetry was performed for a 3-cm lesion by applying the semiautomatic software tool to the MPRs generated from data sets acquired with the T1- and PD-weighted TSE sequence.

Lesion size measurement

After MR measurement, each specimen was cut along its electrode track. This axis of the induced RF necrosis was defined as the *x*-axis. The diameter perpendicular to the cutting plane was defined as the *y*-axis. The *z*-axis was defined perpendicular to the *x*- and *y*-axes.

To validate the MR-based measurement and to determine which of the three histological ablation zones are visualized by MRI, actual diameters of the necrosis zone were measured for the carbonization zone plus the coagulation zone (zones I and II) and for all three zones (zones I–III) (see Figure 2 for the different ablation zones).

As several studies [21, 30] investigated the tissue condition between the coagulation zone next to the RF needle and the pink rim around the lesion detected irreversible cell death and hepatocyte atrophy, we included the transitional zone (TZ) in calculating the ablated volume.

Calculation

For manual calculation of the volume in MRI and macroscopic sections, the following formula was used: $\frac{1}{6}\pi\ (xyz)$.

The percentage deviation of the MRI volumes from the macroscopic volumes was calculated as $\frac{\text{actual volume} - \text{MR volume}}{\text{actual volume}} \cdot 100$.

From correlation of MRI-based and macroscopic measurement, a correction factor (CF) was calculated for estimating actual necrosis volume by MRI: $\frac{\text{actual volume}}{\text{MR volume}} = \text{CF}$.

Statistical analysis

Descriptive statistical data are presented as mean±standard deviation (SD) and include diameters in the *x*-, *y*-, and *z*-axes. RFA volumes were measured by MRI and macroscopically. For volume calculation, the above-mentioned formula was used.

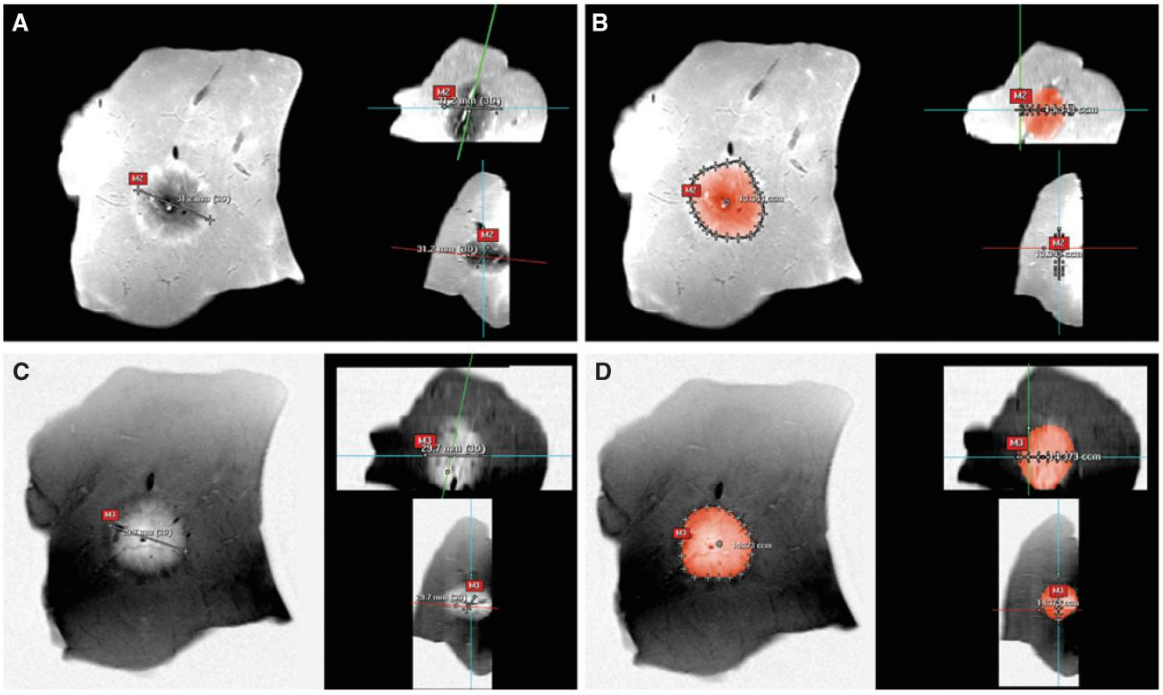

Figure 1: MR volumetry of a 3-cm lesion using semiautomatic software after MPR.
(Top) Diameter measurement (A) and MR volumetry (B) on the MPRs of the data set acquired by T1-weighted sequence. (Bottom) Diameter measurement (C) and MR volumetry (D) of the same lesion on the MPRs of the data set acquired by PD TSE sequence.

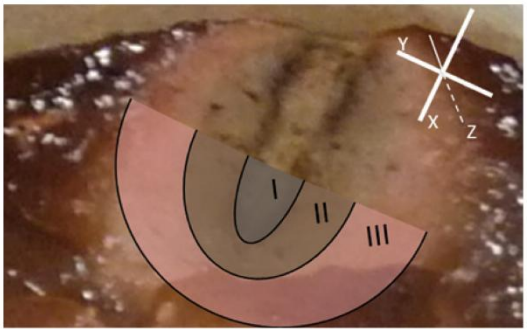

Figure 2: Lesion size measurement and necrosis zones: (I) necrosis/carbonization zone, (II) coagulation zone, and (III) transitional zone. The coordinate system in the upper right aspect indicates the three spatial dimensions for volume calculation.

Spearman's correlation coefficient for association between quantitative variables was used. For paired samples, a Wilcoxon test was performed. p-Values ≤ 0.05 (two-sided) are considered significant. No Bonferroni correction has been performed.

IBM SPSS® Statistics software, version 19.01 (IBM, Armonk, NY, USA), was used for all statistical analysis.

Results

The coagulation necroses were homogenous for all generators and probes. The results obtained with the four systems are summarized in Table 2 for the 3-cm target lesion size and in Table 3 for the 5-cm target lesion size.

Figure 3 depicts macroscopic image validation after RFA with MR correlates.

Radionics

With the Radionics system for the 3-cm lesion, a mean manually measured volume including the TZ of 28.2±6.5 ml was calculated. The volume excluding the TZ was 9.8±3.7 ml. With the T1-weighted sequence, an average volume of 15.2±2.3 ml was detected. This corresponds to a percentage deviation between MR volumetry and manual measurement of 46.1%. Therefore, a correction factor of 1.88 was calculated. With the PD sequence, an average volume of 13.4±3.0 ml was detected. The percentage deviation between MR volume calculation and manual measurement was 52.5%, resulting in a correction factor of 2.13.

For the 5-cm lesion, the manually measured macroscopic volume including the TZ was 48.3±9.9 ml. The calculated volume excluding the TZ was 19.3±7.5 ml. With the T1-weighted sequence, an average volume of 16.4±3.4 ml was detected. In comparison to the manually measured volume including the TZ, a percentage deviation of 66.0% was calculated, resulting in a correction factor of 2.95. With the PD sequence, an average volume of 15.6±3.6 ml

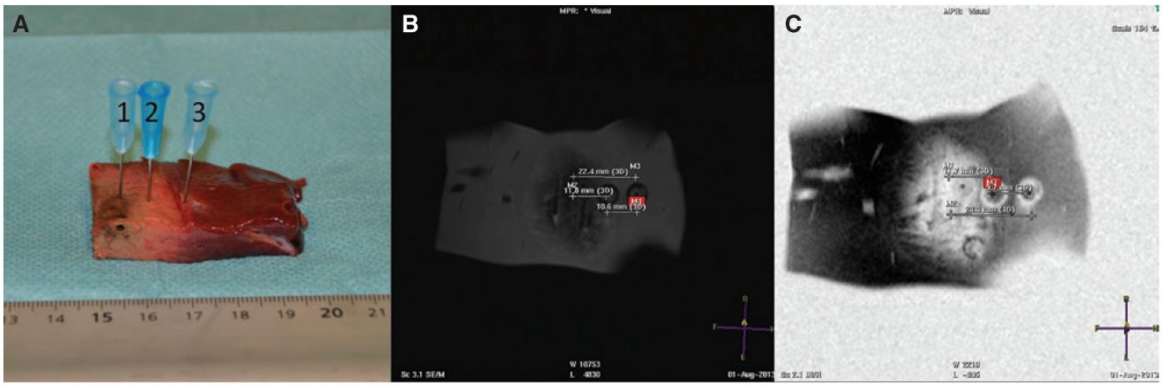

Figure 3: Macroscopic image validation after RFA with MR correlates.
(A) For illustration, a quarter of a 1-cm slice of liver sample including the ablation area is shown. For orientation, cannulas are placed at the macroscopically visible borders of the zones: cannula 1 marks the outer border of the carbonization zone; cannula 2, the outer border of the coagulation zone; cannula 3, the outer border of the transitional zone. (B) MPR of T1-weighted MR image for semiautomatic diameter measurement. (C) MPR of PD-weighted TSE MR image for semiautomatic diameter measurement. M1 and M4 represent the width of the transitional zone (T1, 10.6 mm; PD, 10.7 mm); M2 and M5, the distance from the center of the necrosis to the inner circumference of the transitional zone (T1, 11.8 mm; PD, 11.8 mm); M3 and M6, the distance from center of the necrosis to the outer circumference of the transitional zone (T1, 22.4 mm; PD, 22.5 mm).

was detected, with a percentage deviation (MR vs. manual measurement) of 67.7% and a correction factor of 3.10.

AngioDynamics

For the 3-cm lesion, an average manually measured and calculated volume including the TZ of 17.1±4.9 ml was identified. The volume excluding the TZ was 5.5±3.5 ml. With the T1-weighted sequence, an average volume of 6.3±2.3 ml was detected. The percentage deviation between MRI and the manual measurement including the TZ was 63.2%, resulting in a correction factor of 2.71. Using the PD sequence, an average volume of 6.1±1.6 ml was detected. The percentage deviation was 64.6%, and a correction factor of 2.80 was calculated.

For the 5-cm lesion, the macroscopically calculated volume including the TZ was 39.4±16.2 ml; the volume excluding the TZ was 11.5±6.9 ml. Using the T1-weighted sequence, an average volume of 16.7±6.2 ml was detected, whereas the volume using the PD sequence was 15.2±6.3 ml. The percentage deviation for the T1-weighted sequence was 57.5% versus 61.3% for the PD sequence. The correction factors were 2.36 (T1) and 2.60 (PD).

Boston Scientific

For the 3-cm lesion, the calculated volume including the TZ was 29.7±11.7 ml. The volume excluding the TZ was 17.5±10.8 ml. Using the T1-weighted sequence, an average volume of 12.9±6.5 ml was detected. The percentage deviation (volume including TZ vs. MR) was 56.6%, resulting in a correction factor of 2.30. With the PD sequence, an average volume of 11.5±6.0 ml was detected, with a percentage deviation of 61.3% and a correction factor of 2.58.

For the 5-cm lesion, the volume including the TZ was 71.8±14.5 ml. The calculated volume excluding the TZ was 26.6±8.4 ml. Using the T1-weighted sequence, an average volume of 29.6±6.9 ml was detected. In comparison to the manually measured volume including the TZ, a percentage deviation of 58.8% was calculated, resulting in a correction factor of 2.43. With the PD sequence, an average volume of 27.4±7.2 ml was detected with a percentage deviation of 61.8% and a correction factor of 2.61.

Celon

The average volume for the 3-cm lesion including the TZ with the Celon System was 28.8±7.0 ml, whereas the volume excluding the TZ was 9.7±3.6 ml. Using the T1-weighted sequence, an average volume of 11.3±5.2 ml was detected. In comparison to the manual measurement, the percentage deviation was 60.6%, resulting in a correction factor of 2.55. For the PD sequence, an average volume of 12.8±2.7 ml with a percentage deviation of 55.4% and therefore a correction factor of 2.25 was detected and calculated.

For the 5-cm lesion, an average volume for the lesion including the TZ was 93.3±28.1 versus 42.7±24.5 ml for the lesion excluding the TZ. In comparison to the manual measurement, the average volume using the T1-weighted sequence was 42.6±20.4 ml with a percentage deviation of 54.6% and a correction factor of 2.20. Using the PD sequence, the average volume was 37.5±15.0 ml, resulting in a percentage deviation of 60.1% and a correction factor of 2.50.

Statistical findings

The MRI-derived ablation volumes correlated highly significantly with the volume including the TZ and did not correlate significantly with the volume excluding the TZ. Also, parts of the TZ were detectable by MRI directly after RFA but not consistent for all generators and sizes. For the 3-cm lesion, the correlation of the MR-derived volume with the volume including the TZ was higher than with the volume excluding the TZ. However, the coefficient of correlation was unsatisfactory at 0.621 (PD sequence) and 0.592 (T1-weighted sequence) ($p \leq 0.01$ for both values). For the 5-cm lesion, correlation of the MR-derived volume with the volumes including TZ was 0.903 for the T1-weighted sequence and 0.893 for the PD sequence ($p \leq 0.01$ for both values).

The MR volumes corresponded better with the values of the manually measured volume excluding the TZ (see Tables 2 and 3). Especially for the 5-cm lesion, the PD sequence seems to match with the volume excluding TZ better than the T1 sequence.

Statistically significant differences between MR volumes and manually measured volumes including TZ were detected ($p<0.001$ for all sizes and sequences).

To prove the correctness of our macroscopic volume calculations, the same formula for volume calculation was used for a volume calculation by diameters of the *x*-, *y*-, and *z*-axes in MR. We found a highly significant correlation ($p \leq 0.01$) between the MR volume estimated by semiautomatic software and the volume calculated from diameters measured on MR MPRs. For the T1-weighted sequence, the correlation was 0.888, and for the PD sequence, 0.875.

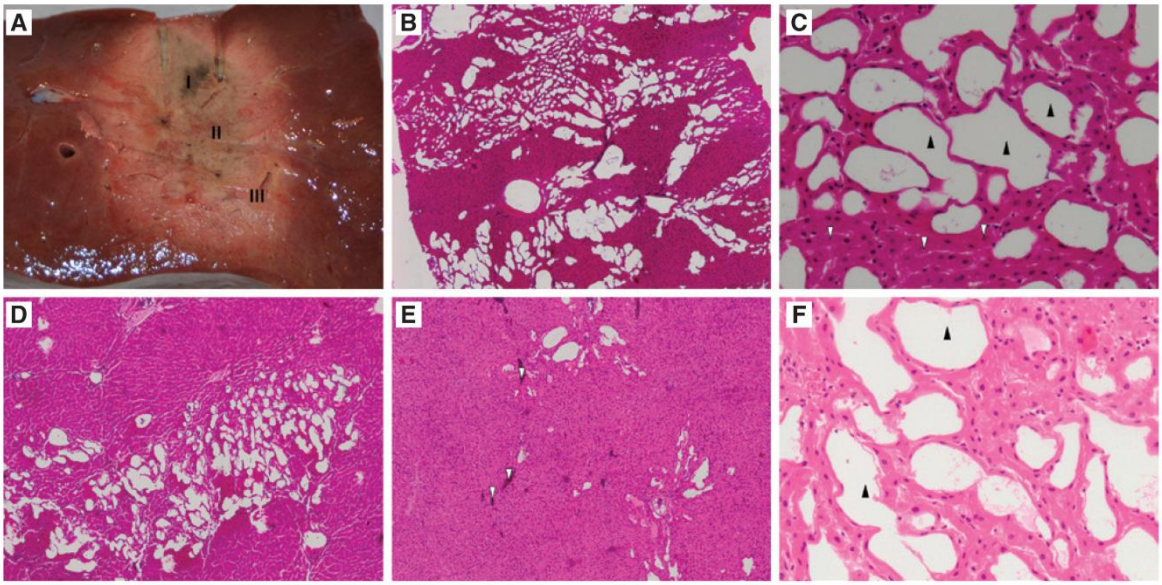

Figure 4: Histopathological correlation of the necrosis zone after ablation.
(A) Transected liver specimen after RFA using two bipolar electrodes (Celon ProSurge). Macroscopic image including zones I–III: (B) microscopic image of zone I (carbonization zone), 40× magnification, showing cauterization artifacts around the electrode track; (C) 200× magnification of zone I (see loss of nuclei, marked by white arrowheads, and pseudocystic cells, marked by black arrowheads); (D) microscopic image of zone II (coagulation zone), 40× magnification, with partial tissue loss and pseudocystic cells; (E) microscopic image of zone III (transitional zone), 40× magnification, with congested blood vessels (white arrowheads); (F) 200× magnification of zone III with scattered pseudocystic cells (black arrowheads); (B–F) hematoxylin and eosin stain (HE).

Histopathological findings

Histopathological workup of one specimen after ablation revealed cautery artifacts around the electrode track with a loss of nucleoli. Furthermore, as shown in Figure 4, a pseudocystic pattern, surrounded by cells with extended nuclei, is apparent. With increasing distance from the necrosis center and decreasing temperature, the number of pseudocystic cells, resulting from strong heat exposure, decreases. In the TZ (Figure 4E), congestion in hepatic blood vessels is detectable.

Discussion

In the clinical setting, when patients are treated by RFA, it is not possible to evaluate treatment outcome by histological examination of the necrosis zone. Therefore, imaging modalities such as CT, MRI, or US are used to evaluate the size and shape of the necrosis in comparison to the pre-ablation images and to determine whether RFA has been successful.

MR volumetry vs. manual measurement

In our experiments, each liver specimen was imaged approximately 10 min after RFA down-cooling. Following MRI, the specimen was dissected for macroscopic validation of the necrosis zone and its shape visualized by MRI. As the correlation between the semiautomatic acquired MR volume and calculated MR MPR diameter volume is highly significant, it seems reasonable to use the above-mentioned formula for volume calculation after macroscopic diameter measurement.

As shown in Tables 2 and 3, MR volumetry consistently yielded smaller ablation volumes than manual measurement after dissection, irrespective of the RF system used, the target lesion size, and the MR sequence. Our data suggest that using the T1-weighted sequence, only about 43.3% of the 3-cm lesion (100–56.7%; see footnote b in Tables 2 and 3) and 40.8% of the 5-cm lesion are visualized. With the PD sequence, about 41.5% of the 3-cm lesion and 37.2% of the 5-cm necrosis volume are detected. Possible explanations for this discrepancy may be a lower temperature in the outer part of the necrosis zone, thereby leading to a lower loss of intracellular and

intraparenchymal water. This may lead to an only partial or a missing signal change in MRI in the outer part of the RF necrosis zone. Also, the relatively low magnetic strength of the MRI system may impede a more accurate evaluation of tissue change.

Several investigators performed MRI using liver-specific contrast agents such as ferucarbotran and gadoxetic acid to differentiate healthy liver from pathological or ablated tissue [13]. The use of liver-specific contrast agents allows an assessment of the outer parts of the necrosis zone in an open 1.0-T MRI system [8]. As the infrastructure to create an accurate perfusion model was not given in our setting, we opted that the use of contrast agents without the guarantee of uniform contrast agent distribution would rather distort imaging than be value adding.

MR sequences and visibility of the TZ

Evaluation of the TZ of ablation after interventional RFA is an ambitious and error-prone task using a 1.0-T open MRI system. The challenge is to visualize and identify the entire TZ after RFA with the MR pulse sequences used for post-interventional imaging. In the outer part of the necrosis zone, the temperature during RFA is not as high as in the coagulation zone. The local temperature is around 100°C at the needle tip of the electrode and decreases with the distance from the electrode. Exposure of tissue to 50°C for 2 min is expected to produce irreversible cellular damage [20, 24]. This corresponds to the outer part of the TZ, which extends to the hemorrhagic rim.

Compared to the visible cellular damage (i.e., loss of core structure), at least in parts of the histological sample, in the carbonization and coagulation zone, it seems to take longer for tissue conversion or connective tissue remodeling to occur in the TZ.

Similar to the study of Lee et al. [14], the TZ remains iso-intense in a hyperacute phase of MRI. Therefore, these changes may not be detectable when MRI is performed immediately after the intervention (compare Figure 3). One reason might be the lack of significant changes in the tissue water content and therefore, caused by the field strength of the MRI, non-visibility of the entire TZ.

With the sequences used in our experiments, the pink rim (i.e., the outer border of the TZ) is not itself visible; however, its extension can be estimated under certain restrictions. We obtained more accurate results in relation to the manually measured volume for the T1-weighted sequence than for the PD sequence. Using correction factors mathematically calculated for specific MR pulse sequences and RF systems and different target ablation volumes may improve the assessment of true ablation volumes for experimental *ex vivo* studies.

It seems reasonable to assume that it is not (yet) possible to see the necrosis shape and diameter in its entirety with the respective MR sequences used. Hence, because ablation volumes were also assessed macroscopically (and its three ablation zones were assessed histopathologically), we are proposing a correction factor as a "workaround" method to approximate the actual size of the ablation volume: i.e., by multiplying the respective ablation volume detected in the respective MRI sequence with the respective correction factor. Also, if the ablation volume after multiplication with the correction factor does not achieve the expected extent, this may serve as an indicator that RFA was insufficient. However, it seems necessary to state that it may not be legitimate to simply transfer this result to an *in vivo* setting, as the correction factor was derived from an *ex vivo* trial.

Volume and size variation of the TZ

As expected, the proportion of the TZ tends to increase with the size of the target ablation volume. In a 3-cm ablation volume, the TZ accounts for an average of 63.9% of the coagulation necrosis (range, 55.9–67.8% for the four RF systems used). For the 5-cm lesion, the TZ makes up an average of 61.9% of the entire coagulation necrosis (range, 54.5–70.1%).

For the AngioDynamics and Boston Scientific system, the proportion of the TZ increases with the ablation volume, unlike for the Radionics and the Celon system, where the TZ shrinks. For the Celon generator, the TZ shrinks from 66.6% (3-cm ablation) to 54.5% (5-cm ablation); for the Radionics system, the TZ shrinks from 65.2 to 59.8%. This might be due to the higher energy output by the cluster electrode during intervention because three electrodes are in use. Also, differences in electrode positioning for the Celon System may result in an expansion of the coagulation zone (see Figure 1): as explained above, to create the 5-cm lesion, three electrodes were positioned in a triangular configuration compared to two electrodes in a line for the 3-cm lesion. Synergistic effects of heat trapping between electrodes have already been described [3]. Current flow between the electrodes as well as a longer ablation time in comparison to the other generators might cause a greater coagulation necrosis zone and therefore a smaller TZ.

Histopathological assessment

It must be noted that even with the histopathological assessment performed here, definitive evidence of complete cell death is difficult to obtain directly after RFA. This is partially attributable to the fact that we used a non-perfused *ex vivo* model without accounting for cellular rebuilding, tissue remodeling, or apoptotic processes. Also, there exist many other more elaborate methods to histopathologically validate cell death, such as nicotinamide adenine dinucleotide (NADH) diaphorase staining kits aimed at validating enzyme activity [18, 19].

Our observations are consistent with published studies. Lee et al. [14] described a similar cellular situation directly after RFA in *in vivo* rabbit liver. They studied the histological effects on liver tissue over time, confirming complete necrosis in the TZ during the follow-up period of 7 weeks after RFA. As the technique of RFA we used is the same as the one used by Lee et al. and former studies confirmed its therapeutic effectiveness, we assume that irreversible cellular damage has been induced in the ablation zone measured in our experiments.

Limitations

Several limitations of this study have to be mentioned. Our experimental data do not reflect ablation volumes in patients. For instance, the heat sink effect of flowing blood results in smaller ablation diameters and volumes after RFA [11, 17]. This was not simulated in our study design, and the lack of heat sink may result in a greater necrosis volume in an *ex vivo* study, as would expected under *in vivo* conditions. Also, RFA was performed in healthy liver tissue and not in tumor tissue. Tumors may contain necrotic areas, and tissue conditions may differ (e.g., tissue effects due to cirrhosis, chemotherapy, dehydration), which may result in lower energy deposition and higher impedance during interventions. All these factors might contribute to smaller ablation volumes *in vivo* than might be expected from our experimental results.

Whereas Breen et al. [4, 5] stated the possibility of total ablation detectability after hyperacute MRI (lesions were induced in rabbit thigh muscle with an optimized macroscopic measurement and data evaluation system), our data suggest that in our non-perfused model, it is not possible to detect the entire necrosis volume directly after intervention. Differences in perfusion (i.e., the absence of perfusion in our model with the consecutive absence of parenchymal heat sink due to blood flow) and differences in tissue conditions (i.e., healthy tissue in contrast to tissue of a real patient with, e.g., cirrhosis and fibrotic restructuration) may result in greater ablation volumes than expected under *in vivo* therapeutic conditions: For example, Stippel et al. [29] argue that the parenchymal restructuring in cirrhotic liver may also induce a heat trapping effect and hence a greater ablation zone than might have been expected. A potential reason for the non-visibility of the TZ after intervention under *ex vivo* conditions in our model may be the absence of a reactive edema and consecutive proton excess in the TZ by means of an inflammation reaction to the thermal injury [32].

Our tests were performed in an open MRI system at 1.0 T, evaluating two different MR sequences. The results in terms of visualization of ablation may be different when MRI is performed on different MR systems with different magnetic strengths and with various sequences; however, as Schraml et al. [26] assessed, there seem to be no significant differences in volumes and shapes between RFAs performed outside and inside the static magnetic field environment. The rationale for using an open MRI system was that MR-guided RFA with near-real-time image guidance (possibly with MR thermometry) may become feasible in the future.

Conclusion

MR volumetry yielded smaller volumes than manual measurement after dissection, irrespective of the RF system used, the target lesion size, and the pulse sequences used.

The full extent of the RF-induced necrosis may not become visible on MR images until full tissue remodeling after the heat-based apoptotic process has occurred for *in vivo* RFA – tissue remodeling is absent in *ex vivo* tissue anyway. This must be kept in mind when using MRI for evaluating outcome directly after RFA without using contrast agents.

We recommend further research for this imaging modality, especially an *in vivo* animal trial or the usage of a tumor model to eliminate interferences. By processing these data, a more accurate statement of expected ablated liver tissue might be possible, also taking into account factors like perfusion and tumor consistency. The performance and processing of near-real-time thermometry during intervention may be able to give a clear statement about the induced necrosis of the TZ directly after ablation, if the use of contrast agents is contraindicated.

Acknowledgments: This research was kindly supported by the TSB – Technology-Foundation Berlin and the European Union (EU) – Fund for regional development. Thank you for you great work! We hope we worked out the comments to your satisfaction. Please feel free to contact us in any kind of further suggestions.

References

[1] Aliberti C, Soriani M, Tilli M, et al. Radiofrequency ablation of liver malignancies: MRI for evaluation of response. J Chemother 2004; 16 (Suppl 5): 79–81.

[2] Assumpcao L, Choti M, Pawlik TM, et al. Functional MR imaging as a new paradigm for image guidance. Abdom Imaging 2009; 34: 675–685.

[3] Brace CL, Sampson LA, Hinshaw JL, et al. Radiofrequency ablation: simultaneous application of multiple electrodes via switching creates larger, more confluent ablations than sequential application in a large animal model. J Vasc Interv Radiol 2009; 20: 118–124.

[4] Breen MS, Lancaster TL, Lazebnik RS, et al. Three-dimensional method for comparing in vivo interventional MR images of thermally ablated tissue with tissue response. J Magn Reson Imaging 2003; 18: 90–102.

[5] Breen MS, Lazebnik RS, Fitzmaurice M, et al. Radiofrequency thermal ablation: correlation of hyperacute MR lesion images with tissue response. J Magn Reson Imaging 2004; 20: 475–786.

[6] Delis S-G. Selection criteria for liver resection in patients with hepatocellular carcinoma and chronic liver disease. World J Gastroenterol 2008; 14: 3452.

[7] Ferlay J, Shin HR, Bray F, et al. Estimates of worldwide burden of cancer in 2008: GLOBOCAN 2008. Int J Cancer 2010; 127: 2893–2917.

[8] Fischbach F, Lohfink K, Gaffke G, et al. Magnetic resonance-guided freehand radiofrequency ablation of malignant liver lesions: a new simplified and time-efficient approach using an interactive open magnetic resonance scan platform and hepatocyte-specific contrast agent. Invest Radiol 2013; 48: 422–428.

[9] Forner A, Bruix J. The size of the problem: clinical algorithms. Dig Dis 2013; 31: 95–103.

[10] Forner A, Llovet JM, Bruix J. Hepatocellular carcinoma. Lancet 2012; 379: 1245–1255.

[11] Goldberg SN, Charboneau JW, Dodd GD 3rd, et al. Image-guided tumor ablation: proposal for standardization of terms and reporting criteria. Radiology 2003; 228: 335–345.

[12] Kim Ys, Lee WJ, Rhim H, et al. The minimal ablative margin of radiofrequency ablation of hepatocellular carcinoma (>2 and <5 cm) needed to prevent local tumor progression: 3D quantitative assessment using CT image fusion. Am J Roentgenol 2010; 195: 758–765.

[13] Koda M, Tokunaga S, Miyoshi K, et al. Assessment of ablative margin by unenhanced magnetic resonance imaging after radiofrequency ablation for hepatocellular carcinoma. Eur J Radiol 2012; 81: 2730–2736.

[14] Lee JD, Lee JM, Kim SW, et al. MR imaging-histopathologic correlation of radiofrequency thermal ablation lesion in a rabbit liver model: observation during acute and chronic stages. Korean J Radiol 2001; 2: 151–158.

[15] Lee MW, Rhim H, Cha DI, et al. Percutaneous radiofrequency ablation of hepatocellular carcinoma: fusion imaging guidance for management of lesions with poor conspicuity at conventional sonography. AJR Am J Roentgenol 2012; 198: 1438–1444.

[16] Lee DH, Lee JM, Lee JY, et al. Radiofrequency ablation for intrahepatic recurrent hepatocellular carcinoma: long-term results and prognostic factors in 168 patients with cirrhosis. Cardiovasc Interv Radiol 2014; 37: 705–715.

[17] Lu DS, Raman SS, Vodopich DJ, et al. Effect of vessel size on creation of hepatic radiofrequency lesions in pigs: assessment of the “heat sink” effect. AJR Am J Roentgenol 2002; 178: 47–51.

[18] Marcovich R, Aldana JP, Morgenstern N, et al. Optimal lesion assessment following acute radio frequency ablation of porcine kidney: cellular viability or histopathology? J Urol 2003; 170: 1370–1374.

[19] Mutsaerts EL, Van Coevorden F, Krause R, et al. Initial experience with radiofrequency ablation for hepatic tumours in the Netherlands. Eur J Surg Oncol 2003; 29: 731–734.

[20] Nath S, Lynch C 3rd, Whayne JG, Haines DE. Cellular electrophysiological effects of hyperthermia on isolated guinea pig papillary muscle. Implications for catheter ablation. Circulation 1993; 88: 1826–1831.

[21] Okubo H, Kokubu S, Komiyama M, et al. Radiofrequency ablation of hepatocellular carcinoma: the feasibility of magnetic resonance imaging with gadolinium ethoxybenzyl diethylene triamine pentaacetic acid for evaluating the ablative margin. Hepatol Res 2010; 40: 1034–1041.

[22] Okusaka T, Okada S, Ueno H, et al. Satellite lesions in patients with small hepatocellular carcinoma with reference to clinicopathologic features. Cancer 2002; 95: 1931–1937.

[23] Parkin DM, Bray F, Ferlay J, Pisani P. Global cancer statistics, 2002. CA Cancer J Clin 2005; 55: 74–108.

[24] Pereira PL, Trubenbach J, Schmidt D. Radiofrequency ablation: basic principles, techniques and challenges. Rofo 2003; 175: 20–27.

[25] Rathke H, Hamm B, Guttler F, et al. Comparison of four radiofrequency ablation systems at target volumes of 3 and 5 cm in an ex vivo bovine liver model. Diagn Interv Radiol 2014; 20: 251–258.

[26] Schraml C, Aube C, Graf H, et al. MR-guided radiofrequency ablation: do magnetic fields influence extent of coagulation in ex vivo bovine livers? Radiology 2006; 241: 746–752.

[27] Schumann C, Bieberstein J, Braunewell S, et al. Visualization support for the planning of hepatic needle placement. Int J Comput Assist Radiol Surg 2012; 7: 191–197.

[28] Smith S, Gillams A. Imaging appearances following thermal ablation. Clin Radiol 2008; 63: 1–11.

[29] Stippel DL, Brochhagen HG, Arenja M, et al. Variability of size and shape of necrosis induced by radiofrequency ablation in human livers: a volumetric evaluation. Ann Surg Oncol 2004; 11: 420–425.

[30] Streitparth F, Knobloch G, Balmert D, et al. Laser-induced thermotherapy (LITT) –evaluation of a miniaturised applicator and implementation in a 1.0-T high-field open MRI applying a porcine liver model. Eur Radiol 2010; 20: 2671–2678.

[31] Venook AP, Papandreou C, Furuse J, de Guevara LL. The incidence and epidemiology of hepatocellular carcinoma: a global and regional perspective. Oncologist 2010; 15 (Suppl 4): 5–13.

[32] Vossen JA, Buijs M, Kamel IR. Assessment of tumor response on MR imaging after locoregional therapy. Tech Vasc Interv Radiol 2006; 9: 125–132.

PUBLIKATION III

Diagn Interv Radiol 2013; 19:427-432
© Turkish Society of Radiology 2013

INTERVENTIONAL RADIOLOGY
ORIGINAL ARTICLE

Fluid preinjection for microwave ablation in an *ex vivo* bovine liver model assessed with volumetry in an open MRI system

Federico Collettini, Hendrik Rathke, Bernhard Schnackenburg, Andreas Thomas, Liane Albrecht, Britta Suttmeyer, Martin Jonczyk, Felix Guettler, Ulf Teichgräber, Thomas Kröncke, Bernd Hamm, Maximilian de Bucourt

PURPOSE
We aimed to detect possible differences in microwave ablation (MWA) volumes after different fluid preinjections using magnetic resonance imaging (MRI).

MATERIALS AND METHODS
MWA volumes were created in 50 cuboid *ex vivo* bovine liver specimens (five series: control [no injection], 10 mL water, 10 mL 0.9% NaCl, 10 mL 6% NaCl, and 10 mL 12% NaCl preinjections; n=10 for each series). The operating frequency (915 megahertz), ablation time (7 min), and energy supply (45 watts) were constant. Following MWA, two MR sequences were acquired, and MR volumetry was performed for each sequence.

RESULTS
For both sequences, fluid preinjection did not lead to significant differences in MWA ablation volumes compared to the respective control group (sequence 1: mean MWA volumes ranged from 7.0±1.2 mm [water] to 7.8±1.3 mm [12% NaCl] vs. 7.3±2.1 mm in the control group; sequence 2: mean MWA volumes ranged from 4.9±1.4 mm [12% NaCl] to 5.5±1.9 mm [0.9% NaCl] vs. 4.7±1.6 mm in the control group). The ablation volumes visualized with the two sequences differed significantly in general ($P < 0.001$) and between the respective groups (control, $P \leq 0.001$; water, $P < 0.001$; 0.9% NaCl, $P < 0.001$; 6% NaCl, $P \leq 0.001$; 12% NaCl, $P < 0.001$). The volumes determined with sequence 1 were closer to the expected ablation volume of 8 mL compared to those determined with sequence 2.

CONCLUSION
For the fluid qualities and concentrations assessed, there is no evidence that fluid preinjection results in larger coagulation volumes after MWA. Because ablation volumes determined by MRI vary with the sequence used, interventionalists should gain experience in how to interpret postinterventional imaging findings (with the MR scanner, sequences, and parameters used) to accurately estimate the outcome of the interventions they perform.

From the Department of Radiology (F.C., H.R., A.T., L.A., B.S., M.J., T.K., B.H., M.D.B. ✉ *mdb@charite.de*), Charité University Medicine, Berlin, Germany; Philips Healthcare (B.S.), Hamburg, Germany; Department of Radiology (F.G., U.T.), Jena University, Jena, Germany.

Received 19 December 2012; revision requested 1 March 2013; revision received 6 March 2013; accepted 21 March 2013.

Published online 5 July 2013.
DOI 10.5152/dir.2013.12189

Thermal ablation techniques are increasingly used in the treatment of various primary and metastatic tumors at different sites, including the liver (1), kidneys (2), and lungs (3). Local ablation is most commonly performed using thermal ablation techniques such as radiofrequency ablation (RFA). Other techniques include laser-induced thermotherapy, cryoablation, high-intensity focused ultrasonography, and microwave ablation (MWA). Local ablation treatment is particularly appealing in combination with image guidance such as ultrasonography, computed tomography, and magnetic resonance imaging (MRI) to allow a minimally invasive approach to therapy (4–8).

Several studies have demonstrated that combining RFA with preinjection of a fluid such as saline (different authors tested a range of concentrations) (9–14) or with diluted hydrochloric acid (15) can yield larger ablation volumes than RFA alone. In addition, both low-field and high-field MRI can be used to monitor the effectiveness of RFA within NaCl-pretreated tissues, and the findings correlate well with pathologic results (9).

Since the advent of MWA, several studies have introduced, tested, and compared this system (16–22), and the legitimate question arose as to whether, with MWA, saline preinjection would also lead to an enlargement of the ablation volume.

Interestingly, to the best of our knowledge, only one study has tested this hypothesis, concluding that preinjected fluids do not enlarge coagulation volumes in MWA (23). That study compared MWA to RFA using default protocols and settings, injecting either 5 mL ethanol, distilled water, 0.9% NaCl solution, or 10% NaCl solution (n=6 each) into *ex vivo* porcine liver (ablations without fluid injection served as the control). Although preinjection of ethanol or 10% NaCl solutions created smaller coagulation volumes, distilled water and 0.9% NaCl solution had no impact.

Hence, initial results indicate that fluid preinjection may not enlarge the ablation volume in MWA, but to the best of our knowledge, it remains unknown whether fluid preinjection in MWA (using different saline concentrations) may affect the appearance of the ablation volume in MRI.

Because a sound understanding of the extent of ablation volumes and ablation margins is imperative for assessing interventional success and successful treatment with MWA, we analyzed whether differences may arise regarding the visualization of MWA volumes with

fluid preinjection using MRI, and in this context, retested whether preinjected fluids enlarge the visualization of coagulation volume in MWA, using our own experimental setup.

Materials and methods

Study design

Our institutional review board approved the present study. MWA ablation volumes were created in 50 cuboid *ex vivo* bovine liver specimens. Five series of 10 repetitions each were conducted as follows: series 1 (n=10, no previous fluid injection as the control group), series 2 (n=10, injection with 10 mL water), series 3 (n=10, injection with 10 mL 0.9% NaCl), series 4 (n=10, injection with 10 mL 6% NaCl), and series 5 (n=10, injection with 10 mL 12% NaCl). After MWA, each specimen was examined with two MRI sequences, and semiautomatic MR volumetry was performed for each sequence (Fig. 1).

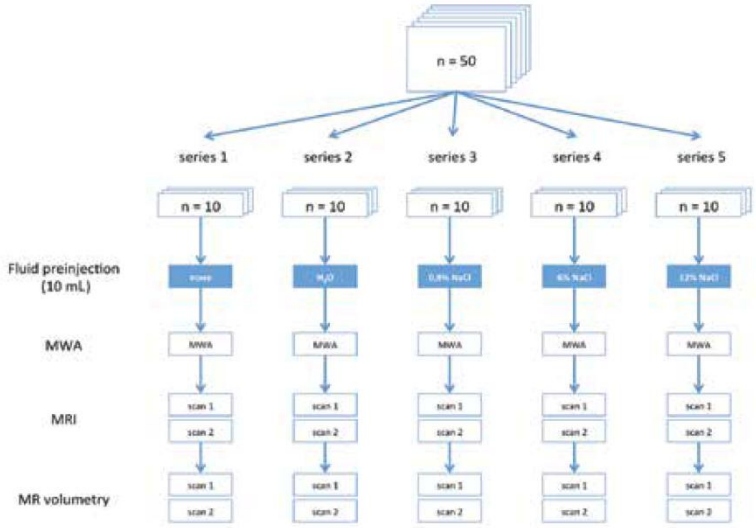

Figure 1. Study design. MRI, magnetic resonance imaging; MWA, microwave ablation.

Liver specimens, storage, and preparation

The *ex vivo* trials were performed with fresh bovine liver provided overnight from a local slaughterhouse. Ten fresh livers including the peritoneum were used. Cuboids of about 8×8×8 cm or larger were created to ensure that the entire coagulation necrosis after each MWA would easily be located inside the parenchyma. Before MWA, all liver specimens were kept in a closed cold chain at <4°C from the time of slaughter to prevent premature denaturation and dehydration. Still-sealed <4°C liver specimens were placed in a plastic tub containing 60 L water and equipped with a heating rod (Eheim Jäger, Deizisau, Germany) with a maximum power of 200 watts (W) and a recirculation pump. The temperature of the recirculating water was set to 37°C to simulate physiological body temperature just before MWA. After reaching physiological body temperature, the specimens were transferred into a kidney basin, and the MWA antenna was maneuvered into the center of the specimen (Fig. 2) and securely fixed. Cuboids of the same bovine liver were used for each run (series 1 to 5) to most accurately ensure comparable tissue conditions of the series.

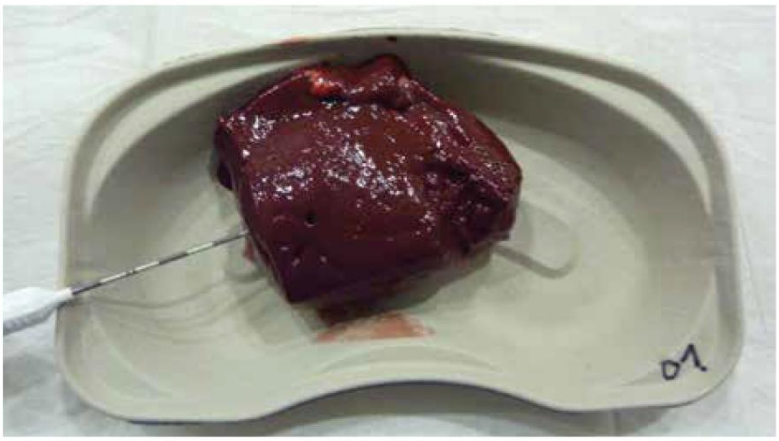

Figure 2. Example of an *ex vivo* bovine liver specimen in a kidney basin with a microwave ablation antenna positioned in the center before microwave ablation.

MWA system, procedure, and semiautomatic volume calculation

The MWA system used consisted of a generator, a pump, and a cart (Evident™ MWA, Covidien, Mansfield, Massachusetts, USA), as well as a percutaneous antenna and pump tubing (Evident™ MWA percutaneous antenna, Covidien). At the operating frequency, the percutaneous antenna delivers electromagnetic waves at 915 megahertz (MHz).

To create ablations, 45 W of power were applied with one antenna for 7 min. All ablations were performed according to the manufacturer's protocol (expected ablation volume with one antenna, 8 mL) and planned with safety margins inside the cuboid liver specimens to ensure that the entire radiating section of

the MWA antenna and the entire consecutive ablation volume would be clearly positioned and measurable inside the cuboid parenchyma. Energy was delivered only when the device was inside the parenchyma. After the preset ablation time was reached, the system shut off automatically.

Immediately after MWA, each liver specimen was scanned in a 1.0 Tesla (T) open MRI system (Panorama HFO, Philips Medical Systems, Best, The Netherlands) with two sequences each (sequence 1: inversion-prepared T1-weighted turbo spin echo [TSE] with inversion prepulse to invert the contrast between the short and long T1 signal, T1-weighted TSE/inversion recovery [IR] [i.e., long T1 appears bright]; sequence 2: pseudo proton-density-weighted TSE; Table 1). Each liver specimen was positioned in a conventional knee coil to obtain a suitable MR signal of the cuboid specimen.

One hundred semiautomatic volumetries were performed (for all 50 MWA ablations and for both MRI sequences) using a semiautomatic volumetric software tool (MR Systems Panorama HFO, Release 2.6.5.0 2009-09-30, Philips Medical Systems).

Statistical analysis

Statistical analysis was performed with paired t tests (with and without Bonferroni adjustment), comparing all MR ablation volumes of sequence 1 with the respective MR ablation volume in sequence 2, individually comparing the respective groups (control, 10 mL water, 10 mL 0.9% NaCl, 10 mL 6% NaCl, and 10 mL 12% NaCl) of the two sequences as well as comparing the respective preinjection groups (10 mL water, 10 mL 0.9% NaCl, 10 mL 6% NaCl, and 10 mL 12% NaCl) in each sequence with its respective control group. For group comparison the dataset was in advance ratified to comply with normality distribution using Kolmogorov-Smirnov test. Statistical analysis was executed using a commercially available software (Statistical Package for Social Sciences for IBM, version 19, release 19.0.0.1, SPSS Inc., Armonk, New York, USA).

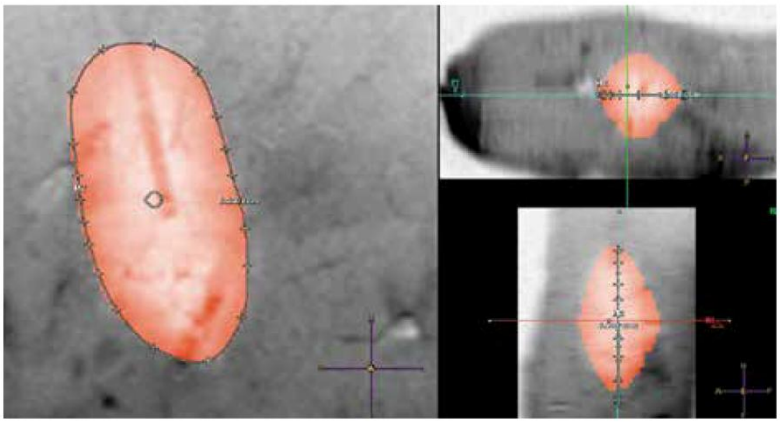

Figure 3. Example of an MR volumetry in coronal, sagittal, and axial views performed for sequence 1 (T1-weighted TSE/IR) with preinjection of 10 mL 6% NaCl. Software tool is MR Systems Panorama HFO (Release 2.6.5.0 2009-09-30, Philips Medical Systems, Best, The Netherlands). Note the filiform signal loss (left) inside the volume, indicating the previous antenna position.

Table 1. MR sequence parameters applied

		Sequence 1 T1-weighted TSE/IR[a]	Sequence 2 PDW TSE[b]
Echo time (ms)		12	30
Repetition time (ms)		800	1800
Inversion time (ms)		50	-
Voxel size (mm)	Foot-head	0.5	0.6
	Right-left	0.6	0.8
Slice thickness (mm)		4	3

[a]Inversion-prepared T1-weighted turbo spin echo sequence with inversion prepulse to invert the contrast between the short and long T1 signal.
[b]Pseudo proton-density-weighted turbo spin echo sequence.

Results

All MW ablations were performed successfully according to the manufacturer's protocol with sufficient safety margins inside the cuboid liver specimens, and all MW ablations were included in the semiautomatic volumetry for both MR scans.

Fig. 3 depicts an example of an MR volumetry performed for sequence 1 (T1-weighted TSE/IR) with preinjection of 10 mL 6% NaCl. Within sequence 1, the fluid preinjection yielded no significant difference in the visualization of the MW ablation volumes compared to the control group without fluid preinjection (Tables 2 and 3). The mean MWA volumes ranged from 7.0±1.2 mm (water) to 7.8±1.3 mm (12% NaCl) vs. 7.3±2.1 mm in the control group.

In addition, within sequence 2, fluid preinjection demonstrated no significant difference in the visualization of the MW ablation volumes compared to the control group (Tables 2 and 3). The mean MWA volumes ranged from 4.9±1.4 mm (12% NaCl) to 5.5±1.9 mm (0.9% NaCl) vs. 4.7±1.6 mm in the control group.

There was, however, a significant difference in ablation volume visualization between the two sequences in general ($P < 0.001$), as well as between corresponding groups between the two sequences (Table 4;

control, $P \leq 0.001$; 10 mL water, $P < 0.001$; 10 mL 0.9% NaCl, $P < 0.001$; 10 mL 6% NaCl, $P \leq 0.001$; 10 mL 12% NaCl, $P < 0.001$). The volumes determined with sequence 1 approximated the expected ablation volume of 8 mL (at 45 W, 7 min, and one antenna, according to manufacturer's protocol) closer than sequence 2.

After Bonferroni adjustment, all significant multiple comparisons remained statistically significant.

Discussion

Comparisons of two MRI sequences revealed no significant differences in the visualization of MWA volumes with fluid preinjection compared to the respective control group without preinjection. Hence, for the tested fluid qualities and concentrations assessed by an open MRI system at 1.0 T, our experiments provide no evidence for enlargement of coagulation volumes in MWA with fluid preinjection, and thus confirm those by Ji et al. (23) in that preinjected fluids do not seem to enlarge coagulation volumes created by MWA.

The two MRI sequences and parameters were initially chosen because they had been found before MR volumetry was performed, to clearly delineate the MWA volume from the surrounding tissue in the open 1.0 T MR scanner we used. However, comparison of the semiautomatic MR volumetry results obtained with the two pulse sequences in the present study revealed that sequence 1 approximated the expected ablation volume of 8 mL significantly better than sequence 2. As different MR sequences may visualize the extent of the same ablation volume differently, the difference may be even greater when imaging is performed on different MR scanners. Hence, it may always be helpful for interventionalists to gain experience regarding how to interpret postinterventional imaging results (with the individual MR scanner, sequences, and parameters used) to accurately estimate the outcome of the interventions they perform.

Table 2. MR volumetry of microwave ablation volumes in the different fluid preinjection groups vs. the control group for sequences 1 and 2

Fluid	None (control)	H_20	0.9% NaCl	6% NaCl	12% NaCl
Preinjection volume (mL)	0	10	10	10	10
Microwave ablation volume (ccm)					
Sequence 1	7.3±2.1	7.0±1.2	7.7±1.8	7.4±1.9	7.8±1.3
Sequence 2	4.7±1.6	5.3±1.4	5.5±1.9	5.2±1.3	4.9±1.4

Data are presented as mean±standard deviation.

Table 3. Paired-samples test of MR volumetry of microwave ablation volumes in the different fluid preinjection groups vs. the control group for sequences 1 and 2

	Paired differences					
			Standard	95% Confidence interval of the difference		
	Mean	Standard deviation	error of the mean	Lower	Upper	*P*
Sequence 1						
Pair 1 Control vs. H_20	0.29990	2.48257	0.78506	-1.47602	2.07582	0.711
Pair 2 Control vs. 0.9% NaCl	-0.37320	1.90357	0.60196	-1.73493	0.98853	0.551
Pair 3 Control vs. 6% NaCl	-0.07950	3.23802	1.02395	-2.39584	2.23684	0.940
Pair 4 Control vs. 12% NaCl	-0.49450	2.12461	0.67186	-2.01435	1.02535	0.480
Sequence 2						
Pair 1 Control vs. H_20	-0.60440	2.37339	0.75053	-2.30222	1.09342	0.441
Pair 2 Control vs. 0.9% NaCl	-0.74460	1.64281	0.51950	-1.91980	0.43060	0.186
Pair 3 Control vs. 6% NaCl	-0.51880	2.28404	0.72228	-2.15271	1.11511	0.491
Pair 4 Control vs. 12% NaCl	-0.17000	2.06753	0.65381	-1.64902	1.30902	0.801

Table 4. Paired-samples test of pairwise comparison of corresponding groups in the two sequences

	Paired differences					
			Standard	95% Confidence interval of the difference		
Sequence 1 vs. Sequence 2	Mean	Standard deviation	error of the mean	Lower	Upper	*P*
Pair 1 Control	2.57780	1.62100	0.51261	1.41820	3.73740	0.001
Pair 2 H_20	1.67350	0.61390	0.19413	1.23434	2.11266	< 0.001
Pair 3 0.9% NaCl	2.20640	1.26936	0.40141	1.29836	3.11444	< 0.001
Pair 4 6% NaCl	2.13850	1.45174	0.45908	1.09999	3.17701	0.001
Pair 5 12% NaCl	2.90230	1.42156	0.44954	1.88538	3.91922	< 0.001

Another interesting aspect worth discussing is why the fluids (10 mL water, 10 mL 0.9% NaCl, 10 mL 6% NaCl, and 10 mL 12% NaCl) injected before MWA consistently did not significantly enlarge the ablation volume in our *ex vivo* experiment. Hence, fluid preinjection appears to enhance the effectiveness of RFA but not MWA. This difference may be attributable to different effects of RFA and the microwave technique—with RFA, the amount of heat generated in the target tissue is determined by the amount of current that passes from the electrode through the tissue. Current is defined as the electric charge per unit time (I=Q/t, where I is current in amperes, Q is charge in coulombs, and t is time in seconds)

and heats the tissue via impedance (resistance). Fluids such as saline can lower tissue impedance. The lower the impedance, the more efficiently a generator can deliver the desired current, resulting in more heat per unit time delivered. In addition, saline can effectively increase the size of the electrode, reducing current density at the electrode-tissue interface and the likelihood of high impedance buildup around the electrode. Sustained and higher-power delivery to the tissue results in larger ablation volumes.

Because MWA systems do not rely on electrical impedance to produce heat, saline injection cannot influence energy delivery via that physical mechanism. In other words, saline preinjection should result in about the same heat per unit time as no saline preinjection, or maybe even less (with the possibility of creating a smaller ablation volume): some of the applied MWA heat may be absorbed by saline, reducing the energy reaching the tissue. Furthermore, saline may actually reduce the amount of energy delivered by the antenna due to conductivity: MW energy may reflect a conductive boundary, and saline present at the target site may to some extent block the energy from leaving the probe. Conversely, however, one recent publication has provided initial evidence that extension of microwave coagulation may still be possible using a special perfusion microwave electrode (24).

Our study has several limitations. This was an *ex vivo* study with a small number of MWA treatments performed in the individual fluid preinjection groups and the control group. Although the *ex vivo* setup simulated some physiological conditions (e.g., warming up the fresh bovine liver cuboids to physiological temperature of 37°C just before MWA), other *in vivo* conditions such as vascular perfusion (to account for possible heat-sink effects) were not modeled. In addition, as discussed above, MR visualization of ablation volumes varies with the pulse sequence used and may also differ among MR scanners, manufacturers, and field strengths.

In conclusion, interventionalists must consider the characteristics of ablation volumes when using MWA instead of RFA and when using MRI for visualization and validation of the ablation volumes created.

Acknowledgements

This study was supported by the TSB Technologiestiftung-Zukunftsfonds, Berlin, Germany, and the European Union-European Fund for Regional Development, Berlin, Germany.

Conflict of interest disclosure

The authors declared no conflicts of interest.

References

1. Kuang M, Xie XY, Huang C, et al. Long-term outcome of percutaneous ablation in very early-stage hepatocellular carcinoma. J Gastrointest Surg 2011; 15:2165–2171. [CrossRef]
2. Lee JM, Han JK, Chang JM, et al. Radiofrequency renal ablation: in vivo comparison of internally cooled, multitined expandable and internally cooled perfusion electrodes. J Vasc Interv Radiol 2006; 17:549–556. [CrossRef]
3. Lu Q, Cao W, Huang L, et al. CT-guided percutaneous microwave ablation of pulmonary malignancies: results in 69 cases. World J Surg Oncol 2012; 10:80. [CrossRef]
4. Goldberg SN, Gazelle GS, Mueller PR. Thermal ablation therapy for focal malignancy: a unified approach to underlying principles, techniques, and diagnostic imaging guidance. AJR Am J Roentgenol 2000; 174:323–331. [CrossRef]
5. Keil S, Bruners P, Schiffl K, et al. Radiofrequency ablation of liver metastases-software-assisted evaluation of the ablation zone in MDCT: tumor-free follow-up versus local recurrent disease. Cardiovasc Intervent Radiol 2010; 33:297-306. [CrossRef]
6. Streitparth F, Knobloch G, Balmert D, et al. Laser-induced thermotherapy (LITT)--evaluation of a miniaturised applicator and implementation in a 1.0-T high-field open MRI applying a porcine liver model. Eur Radiol 2010; 20:2671–2678. [CrossRef]
7. Wang Z, Aarya I, Gueorguieva M, et al. Image-based 3D modeling and validation of radiofrequency interstitial tumor ablation using a tissue-mimicking breast phantom. Int J Comput Assist Radiol Surg 2012; 7:941–948. [CrossRef]
8. Haigron P, Dillenseger JL, Luo L, Coatrieux JL. Image-guided therapy: evolution and breakthrough. IEEE Eng Med Biol Mag 2010; 29:100–104. [CrossRef]
9. Nour SG, Goldberg SN, Wacker FK, et al. MR monitoring of NaCl-enhanced radiofrequency ablations: observations on low- and high-field-strength MR images with pathologic correlation. Radiology 2010; 254:449–459. [CrossRef]
10. Lee JM, Kim SH, Han JK, Sohn KL, Choi BI. Ex vivo experiment of saline-enhanced hepatic bipolar radiofrequency ablation with a perfused needle electrode: comparison with conventional monopolar and simultaneous monopolar modes. Cardiovasc Intervent Radiol 2005; 28:338–345. [CrossRef]
11. Shimizu A, Ishizaka H, Awata S, et al. Expansion of radiofrequency ablation volume by saturated NaCl saline injection in the area of vaporization. Acta Radiol 2009; 50:61–64. [CrossRef]
12. Lee JM, Kim YK, Lee YH, Kim SW, Li CA, Kim CS. Percutaneous radiofrequency thermal ablation with hypertonic saline injection: in vivo study in a rabbit liver model. Korean J Radiol 2003; 4:27–34. [CrossRef]
13. Lee JM, Youk JH, Kim YK, et al. Radio-frequency thermal ablation with hypertonic saline solution injection of the lung: ex vivo and in vivo feasibility studies. Eur Radiol 2003; 13:2540–2547. [CrossRef]
14. Iishi T, Hiraki T, Mimura H, et al. Infusion of hypertonic saline into the lung parenchyma during radiofrequency ablation of the lungs with multitined expandable electrodes: results using a porcine model. Acta Med Okayama 2009; 63:137–144.
15. Luo RG, Fao F, Huang JH, Gu YK, Jiang XY, Huang YJ. Diluted hydrochloric acid generates larger radiofrequency ablation lesions in excised porcine livers. Diagn Interv Radiol 2012;19:145–149.
16. Simon CJ, Dupuy DE, Mayo-Smith WW. Microwave ablation: principles and applications. Radiographics 2005; 25(Suppl 1):S69–S83. [CrossRef]
17. Wolf FJ, Aswad B, Ng T, Dupuy DE. Intraoperative microwave ablation of pulmonary malignancies with tumor permittivity feedback control: ablation and resection study in 10 consecutive patients. Radiology 2012; 262:353–360. [CrossRef]
18. Carrafiello G, Laganà D, Mangini M, et al. Microwave tumors ablation: principles, clinical applications and review of preliminary experiences. Int J Surg 2008; 6(Suppl 1):S65–S69. [CrossRef]
19. Hoffmann R, Rempp H, Clasen S. Microwave tumor ablation. New devices, new applications?. Radiologe 2012; 52:22–28. [CrossRef]
20. Livraghi T, Meloni F, Solbiati L, Zanus G, for the Collaborative Italian Group using AMICA system. Complications of microwave ablation for liver tumors: results of a multicenter study. Cardiovasc Intervent Radiol 2012; 35:868–874. [CrossRef]

21. Andreano A, Brace CL. A comparison of direct heating during radiofrequency and microwave ablation in *ex vivo* liver. Cardiovasc Intervent Radiol 2013; 36:505–511. [CrossRef]
22. Bertot LC, Sato M, Tateishi R, Yoshida H, Koike K. Mortality and complication rates of percutaneous ablative techniques for the treatment of liver tumors: a systematic review. Eur Radiol 2011; 12:2584–2596. [CrossRef]
23. Ji Q, Xu Z, Liu G, Lin M, Kuang M, Lu M. Preinjected fluids do not benefit microwave ablation as those in radiofrequency ablation. Acad Radiol 2011; 18:1151–1158. [CrossRef]
24. Umehara H, Seki T, Inokuchi R, et al. Microwave coagulation using a perfusion microwave electrode: Preliminary experimental study using *ex vivo* and *in vivo* liver. Exp Ther Med 2012; 3:214–220.

LEBENSLAUF

ÄRZTLICHE TÄTIGKEIT

STUDIUM

PRAKTISCHES JAHR

Mein Lebenslauf wird aus datenschutzrechtlichen Gründen in der elektronischen Version meiner Arbeit nicht veröffentlicht.

Schulbildung

Kongressbeiträge

Famulaturen und Hospitation

Mein Lebenslauf wird aus datenschutzrechtlichen Gründen in der elektronischen Version meiner Arbeit nicht veröffentlicht.

VOLLSTÄNDIGE PUBLIKATIONSLISTE

9.

Suttmeyer B, Teichgräber U, **Rathke H**, Albrecht L, Guettler F, Schnackenburg B, Hamm B, de Bucourt M.

Initial experience with imaging of the lower extremity arteries in an open 1.0 Tesla MRI system using the triggered angiography non-contrast-enhanced sequence (TRANCE) compared to digital subtraction angiography (DSA).

Biomed Tech (Berl). 2016 Aug 1;61(4):383-92. doi: 10.1515/bmt-2014-0181

8.

Seithe T, Busse R, Rief M, Doyscher R, Albrecht L, **Rathke H**, Jonczyk M, Poschmann R, Tepe H, Hamm B, de Bucourt M.

[Teleradiological report turnaround times: An internal efficiency and quality control analysis]

Radiologe. 2015 May;55(5):409-16. doi: 10.1007/s00117-015-2858-0.

7.

Rathke H, Hamm B, Güttler F, Lohneis P, Stroux A, Suttmeyer B, Jonczyk M, Teichgräber U, de Bucourt M.

„Volume comparison of radiofrequency ablation at 3 cm and 5 cm target volumes for four different RF generators – MR volumetry in an open 1 Tesla MRI system versus macroscopic measurement.“

Biomed Tech (Berl). 2015 Dec 1;60(6):521-31. doi: 10.1515/bmt-2014-0174.

6.

Makowski M, Jonczyk M, Streitparth F, Guettler F, **Rathke H**, Suttmeyer B, Albrecht L, Teichgräber U, Hamm B, de Bucourt M.

„Interactive near-real-time high-resolution imaging for MR-guided lumbar interventions using ZOOM imaging in an open 1.0 Tesla MRI system - initial experience”

Biomed Tech (Berl). 2015 Dec 1;60(6):533-9. doi: 10.1515/bmt-2014-0118.

5.

Rathke H, Hamm B, Güttler F, Rathke J, Rump J, Teichgräber U, de Bucourt M.

„Comparison of four radiofrequency ablation systems at two target volumes in an ex vivo bovine liver model.“

Diagn Interv Radiol. 2014 May-Jun;20(3):251-8. doi: 10.5152/dir.2013.13157.

4.

Suttmeyer B, Teichgräber U, Thomas A, **Rathke H**, Albrecht L, Jonczyk M, Verba M, Güttler F, Schnackenburg B, Hamm B, de Bucourt M.

„Non-invasive ECG-triggered 2D TOF MR angiography of the pelvic and leg arteries in an open 1.0-tesla high-field MRI system in comparison to conventional DSA.“

Biomed Tech (Berl). 2014 Feb;59(1):29-37. doi: 10.1515/bmt-2013-0113.

3.

Jonczyk M, Hamm B, Heinrich A, Thomas A, **Rathke H**, Schnackenburg B, Güttler F, Teichgräber UK, de Bucourt M.

„Initial clinical experience with a quadrupole butterfly coil for spinal injection interventions in an open MRI system at 1.0 tesla.“

Biomed Tech (Berl). 2014 Feb;59(1):39-45. doi: 10.1515/bmt-2013-0066.

2.

Collettini F, **Rathke H**, Schnackenburg B, Thomas A, Albrecht L, Suttmeyer B, Jonczyk M, Guettler F, Teichgräber U, Kroncke T, Hamm B, de Bucourt M.

„Fluid preinjection for microwave ablation in an ex vivo bovine liver model assessed with volumetry in an open MRI system.“

Diagn Interv Radiol. 2013 Sep-Oct;19(5):427-32. doi: 10.5152/dir.2013.12189.

1.

de Bucourt M, Streitparth F, Collettini F, Guettler F, **Rathke H**, Lorenz B, Rump J, Hamm B, Teichgräber UK.

„Minimally invasive magnetic resonance imaging-guided free-hand aspiration of symptomatic nerve route compressing lumbosacral cysts using a 1.0-Tesla open magnetic resonance imaging system.“

Cardiovasc Intervent Radiol. 2012 Feb;35(1):154-60. doi: 10.1007/s00270-011-0120-3. Epub 2011 Mar 9.

DANKSAGUNG

Mein herzlicher Dank gilt meinem Doktorvater und Betreuer Herrn PD Dr. med. Maximilian de Bucourt. Ich möchte mich ganz besonders für seine Geduld und Mitarbeit bei den Versuchen, bei der anschließenden Aufbereitung der Daten und der Ausarbeitungen der Publikationen bedanken. Ohne seine Hilfe und Zutun wäre diese Promotion im diesem Umfang nicht möglich gewesen! Ebenfalls möchte ich mich bei Herrn Professor Dr. med. Ulf Teichgräber bedanken, der als Arbeitsgruppenleiter der AG offene MRT den Grundstein für diese Promotion gelegt hat und bis zu seiner Berufung an das Universitätsklinikum Jena als Doktorvater dieser Promotion vorstand. Ihm gilt mein Dank für die Überlassung des Themas. Ferner gilt mein Dank Herrn Dr. rer. nat. Jens Rump und Herrn Dr. Bernhard Schnackenburg für die sehr gute Unterstützung in der Planungs- und Ausführungsphase der Versuche und der MR-Sequenzen. Auch Herrn Lothar Westhoff gilt mein Dank für die Herstellung der Versuchsapparatur zur Erwärmung der Leberproben. Mein Dank gilt Frau Dipl.-Math. Andrea Stroux aus dem Institut für Biometrie der Charité für die Unterstützung und Beratung hinsichtlich der Fallzahlplanung und der statistischen Auswertung. Herrn Dr. med. Philipp Lohneis danke ich für die histologische Aufarbeitung und Befundung der Leberprobe. Für die Hilfe, sowohl bei der statistischen Auswertung, als auch während des gesamten Promotionsprozesses bedanke ich mich herzlich bei meinem Bruder Dr. nat. techn. Jörn Bernhard Rathke, der mir bei aufkommenden Fragen immer unterstützend zur Seite stand.

Bei meinen Eltern, Kerstin und Bernhard Rathke sowie meinen Großeltern möchte ich mich für die vollumfängliche Unterstützung während des Studiums und der Promotion bedanken. Ebenso für die finanzielle Unterstützung und die Möglichkeit, am Kongress der Society of Interventional Radiology in San Francisco im Jahr 2012 teilnehmen zu können. Ihnen gilt mein herzlicher Dank für alles was sie bisher für mich getan haben! Ich danke meinen Freunden, insbesondere Benjamin Freitag und Dr. med. Christian Oberender für die stets konstruktive Kritik in allen Belangen. Ich danke allen Freunden und Verwandten, die immer wieder für Fragen ein offenes Ohr hatten und mich während der Zeit des Studiums beziehungsweise der Dissertation und darüber hinaus begleitet haben.